Multi-objective optimisation of a solar district heating network with seasonal storage for conditions in cities of southern Chile

Multi-objective optimisation of a solar district heating network with seasonal storage for conditions in cities of southern Chile

Serguey A. Maximov[a,1], Sajid Mehmood[a,b,2], Daniel Friedrich[a,*]

[a] *School of Engineering, Institute for Energy Systems, University of Edinburgh, Colin Maclaurin Road, Edinburgh EH9 3DW, UK*
[b] *Department of Mechanical, Mechatronics and Manufacturing Engineering (New Campus), University of Engineering & Technology, Lahore, Pakistan*

Abstract

Rapid urban growth and enhanced quality of life have significantly increased the demands for indoor heating, especially in the developing world. In Chile, this demand is provided largely through low quality biomass which creates pollution problems. Due to the medium to high solar resource in most of Chile, solar thermal networks with seasonal thermal storage should be considered. In this paper, we assessed the use of solar energy with seasonal thermal energy storage to provide domestic heating through a heat network. For this, we performed a simulation-based multi-objective optimisation of the system's design with cost and greenhouse gas emissions as objectives for two locations in Chile. Our results show that solar thermal networks are

*Corresponding author
Email address: d.friedrich@ed.ac.uk (Daniel Friedrich)

[1]Researcher funded by a PhD Scholarship from ANID PFCHA/DOCTORADO BECAS CHILE/2017—72180200.

[2]Researcher funded by a PhD Scholarship from the Higher Education Commission (HEC)Pakistan and with the support of the University of Engineering and Technology, Lahore, Pakistan.

cost-competitive with conventional alternatives. Furthermore, the inclusion of seasonal thermal storage could improve the system performance decreasing the emissions by around 90% while increasing the $LCOE$ by less than 20% compared with a conventional gas-heated network or resistive electric heating. We found that for specific systems configuration and locations solar district heating with long term storage could be cost-competitive with burning firewood if externalities such as the social costs of local pollution were considered in the economic analysis.
Keywords: District heating, seasonal storage, solar thermal, multi-objective optimisation, genetic algorithm, Chile

1. Introduction

Worldwide, activities in buildings accounts for close to 28% of energy-related greenhouse gas (GHG) emissions and it is estimated that 50 to 60% of these emissions are due to indoor heating and cooling services [1]. In Chile, close to 50% of space heating demand is provided through cheap low-quality biomass [2] and in southern Chile close to 90% of households use firewood stoves for heating [3]. Although biomass produces low GHG emissions, it is the main cause of acute pollution problems in several towns in central and southern Chile and it is responsible for more than 85% of the PM2.5 (fine particulate matter) emissions in Chile [4].

There is a broad consensus that district heating networks in urban areas need to be part of the lowest cost decarbonisation pathway and can significantly reduce local emissions [5, 6, 7]. This is mainly due to the possibility of taking advantage of economies of scale that allow using more efficient tech-

nologies, getting better control of local emissions and integrating cheaper large scale storage to maximise the use of renewable resources. Due to the medium to high solar resource, with global horizontal irradiance ranging between 1,400 and 2,600 kWh/m^2·a in most of Chile [8, 9], solar thermal networks with seasonal thermal storage should be considered as an alternative for reducing GHG emissions and local pollution at affordable costs.

In addition, most households in central and southern Chile do not reach thermal comfort during wintertime, with indoors temperatures often around 15°C [10]. Moreover, the heating requirements are met mostly by burning firewood in stoves (47%) or in individual ventless gas heaters (31%) [2]. This creates a scenario of high levels of pollution indoors [11] and especially outdoors [9], with the city of Coyhaique presenting average concentrations of PM2.5 close to 60 µg/m^3 and Temuco exceeding 45 µg/m^3, while the standard sets a maximum of 20 µg/m^3 [4].

Notwithstanding this complex scenario, the cities of Temuco and Coyhaique have a good relation between annual heat requirements and availability of solar resource. This is expressed in Table 1, where the heating degree days (HDD) and annual global horizontal irradiance (GHI) are compared. From Table 1 it can be noted that this Chilean cities are located in lower latitudes than cities with similar heating demands in Europe. This results in a higher solar resource availability for a given heating requirement, which supports the initial assumptions that there is a good case for solar heating in central and southern Chile.

The annual behaviour of the ambient temperature and the annual variation of the GHI for the cities of study are presented in Figure 1. It shows

Table 1: Comparison of conditions of the analysed locations and cities with similar heating requirements in Europe

	Temuco	Paris	**Coyhaique**	Stockholm	Unit
Latitude	**-38.7**	48.8	**-45.6**	59.3	[°]
Annual HDD (base 15.5°C)	**1,748**	1,743	**2,901**	3,047	[HDD]
Annual GHI	**1,676**	1,405	**1,461**	1,154	[kWh/m²·a]

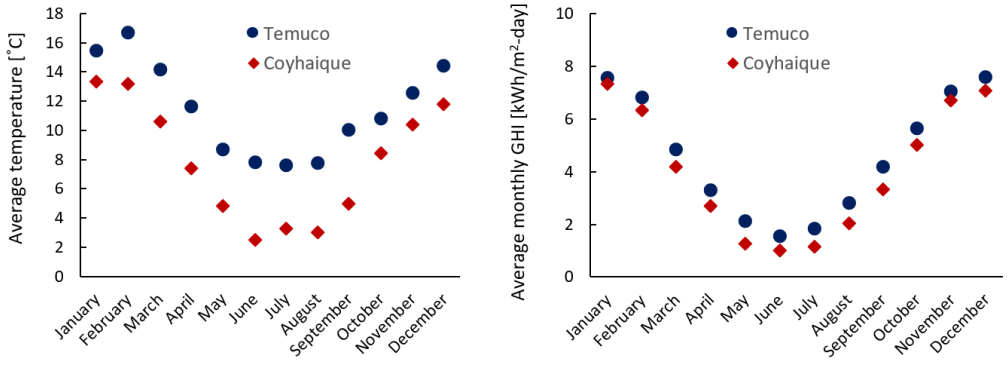

Figure 1: Average daily temperature each month (left). Average daily global horizontal irradiance (GHI) (right)

that the lowest temperature, hence, the highest heating demand are concurrent with the lowest solar energy availability. This means that to be able to supply a high fraction of the thermal demand from solar energy in winter the solar system would certainly be oversized for the rest of the year, which is economically sub optimal. An alternative to this scenario is the option of storing part of the surplus energy available in summer in order to be used in winter by means of seasonal thermal energy storage.

Seasonal thermal energy storage has the capacity of storing solar energy captured in summer to supply winter heating demand, increasing the fraction of the annual heating demand supplied by solar energy, also known as solar fraction (SFr). In order to achieve high storage capacities at an affordable cost, these systems store energy in inexpensive materials, such as water, soil or both. In borehole thermal energy storage (BTES) the soil is used as the storage as well as insulation material: heat dissipates slowly due to the low soil thermal conductivity and a radial horizontal thermal gradient is generated. In order to deliver and retrieve the heat from the soil, vertical holes between 20-100 m deep are drilled in the ground and water carrying U-shaped pipes are inserted in the holes. The hot water supply is connected at the centre of the storage and several holes are connected radially in series forming a string. Several strings are connected in parallel covering the entire volume of the BTES. During the charging of the storage, hot water flows from the centre to the perimeter and the flow is reversed during the discharging to keep the horizontal stratification. Further information and schematics on these systems can be found in Sorensen [12].

District heating networks and, particularly, the integration of seasonal thermal energy storage require sophisticated design and optimisation tools. Many optimisation approaches to thermal networks have focused on exploring mathematical optimisation applied to the design of the network with single objective function, such Krug et al. [13] who perform an non-linear optimisation approach, Blackburn et al. [14] who present a very fast to solve dynamic optimization approach or Romanchenko et al. [15] who performed a mixed-integer unit commitment approach to assess the interactions of a ther-

mal energy storage and demand side response in a district heating network's operation. However, these approaches cannot be used in scenarios when more than one objective function needs to be considered, such as when assessing decarbonisation options at affordable costs, which are essential so that the district heating systems with seasonal thermal energy storage provide both environmental and economic benefits.

In previous research assessing the performance of solar systems with seasonal storage, Renaldi and Friedrich [16] developed a simulation model based on the Drake Landing Solar Community project built in Canada [17]. In their work, they analysed the performance of the system operating under British conditions and performed a sensitivity analysis on some of the main variables. However, no optimisation of the system's configuration was performed. Rehman et al. [18] compared the performance of different designs performing optimisation analysis on centralised and decentralised heating networks. However, the analysis was performed for cold Finish conditions, which differ from the sunny and cool conditions previously described for Chile. Lizana et al. [19] performed a techno-economic analysis for solar heating networks operating in Mediterranean climates, which are similar in solar availability to the Chilean case, but in general present lower heating demands. Shah et al. [20] performed an optimisation of a similar system in various cold climate locations in the northern hemisphere. In their work they carried out a multi-objective optimisation for two design variables of the system and compared their results with several single-objective optimisations. All these studies concluded that low emission solar district networks could be cost-competitive with conventional technologies under certain conditions.

However, no literature has been found on the assessment of the design and operation of these systems in the southern hemisphere, and particularly under the sunny but cool conditions of central and southern Chile. In addition, many of the available optimisation studies for seasonal thermal energy storage systems present only the optimisation results and do not go into detail about the corresponding system configurations. Furthermore, many studies consider only the sizing of the system but not the operational parameters. For example, the authors are not aware of any study investigating the optimal solar collector angle in relation to the design of a district heating system with long term storage. However, this information is essential to enable further improvements and uptake of these systems.

In this work, we assessed the use of solar energy to provide domestic heating for social housing in Chile through a solar-driven heat network with seasonal thermal energy storage. We developed a detailed and fully parametrised TRNSYS simulation model and linked this through a custom Python interface to multi-objective optimisation tools. We used this to perform a simulation-based multi-objective optimisation of the system's design with total costs and GHG emissions as objectives for the cities of Temuco and Coyhaique. Hourly heating loads were estimated for social housing blocks. The variability of internal gains, standard materials, geometry and typical families' occupancy rates were considered. The results of the optimisation present a range of system configurations that minimise the total cost and the GHG emissions. These objective functions are mutually competing; thus, each optimal system configuration presents a trade-off between emissions and cost. We analyse how the main parameters that define the system con-

figuration interact with these trade-offs and explore the effects of location, climate conditions and system size in the optimal solutions and in the competitiveness of the system with conventional heating options. We consider an in depth analysis of the optimal operational temperatures of the district network operating in Chile and include a novel analysis on the effects of optimising the collector tilt angle considering the interaction of the local weather conditions, the shape of the thermal demand and the effects of the long term storage.

2. Methods

In the context of the issues around domestic heating and the solar resource described in the previous section, this paper describes a techno-economic analysis of the use of solar energy to provide domestic heating for two cities in southern Chile.

The general framework of the analysis was a multi-objective simulation-based optimisation with the system's cost and GHG emissions as optimisation objectives. The use of these opposing objectives (as usually a "cleaner" system has a higher cost) allows the assessment of a wide range of optimal solutions that provide a compromise between cost and emission levels. This general framework consists of three main blocks and is presented in Figure 2:

1. Estimation of the heat load during a year for a specific building configuration and location.
2. Simulation of the performance of the system during one or more operational years.

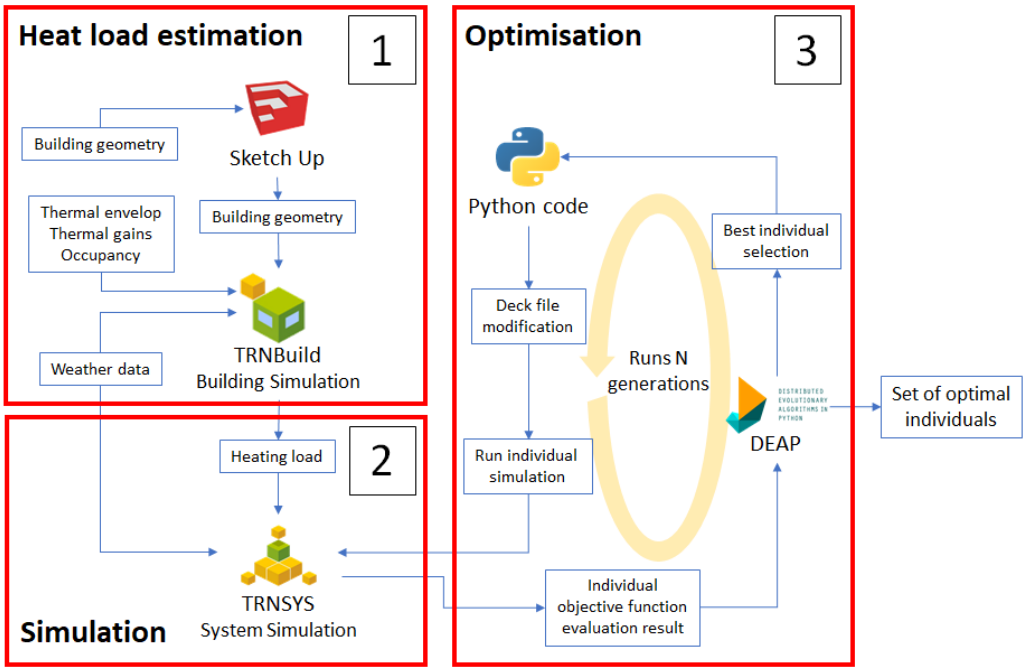

Figure 2: Main framework of the analysis showing the three main blocks: heat load estimation, simulation and optimisation

3. Optimisation of the system configuration for a given heating load and location.

2.1. Heating demand estimation

The heating load was calculated for social housing blocks in the cities of Temuco and Coyhaique. As shown in the first block of Figure 2, the calculation was performed on a multi-zone TRNBuild v3.0 model, which allows the simulation of the independent behaviour of rooms and areas of the flats. The geometry of a standard eight duplex flats block was drawn and imported from SketchUp, as shown in Figure 3. This geometry was based in a block of 8 duplex flats of 51 m^2 each, which emulates social

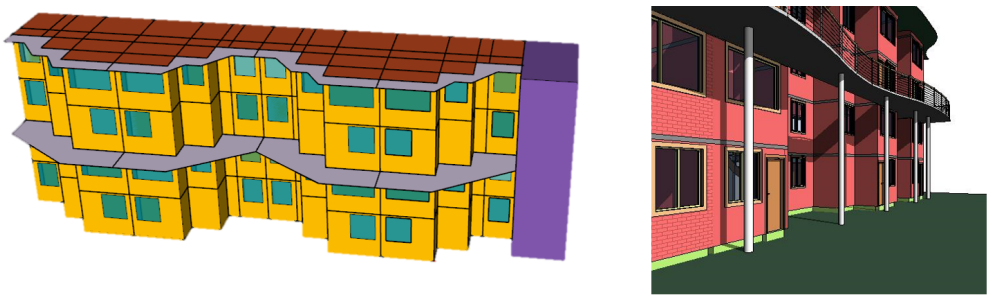

Figure 3: SketchUp model of the buildings (left) and original architectonic design (right)

housing designs at the current thermal standard. Each flat was modelled with six thermal zones. The lower floor was modelled with three zones: hall, kitchen and toilet, while the upper floor was modelled with two zones: main bedroom and secondary bedrooms. The staircase was designed as a sixth zone, thermally connecting both floors.

The geometry of the building was imported into TRNbuild. The materials of the thermal envelope were selected according to the minimum requirements in the Chilean thermal standard from 2007 for each climate zone [21]. The main parameters for each location are shown in Table 2 and the detail of the walls and roof materials considered in the simulation are presented in Appendix A. For the heat gains and heat requirements definition in time an occupancy rate of a typical four people family showed in Figure 4 was assumed.

The control logic of the heating is on-off and it sets the temperature to 21°C when there are occupants in a zone and 16°C when there are no occupants. This applies to the living room and the bedrooms. The kitchen and toilet are kept at 16°C. There is no heating considered for the staircase. Additionally, heat gains were considered due to the presence of active occu-

Table 2: Thermal standards used in the model

City	Thermal zone number	Maximum U [W/m^{2}K]			Max window wall coverage
		Roof	Wall	Floor	
Temuco	5	0.33	1.6	Not defined	18%
Coyhaique	7	0.25	0.6	Not defined	12%

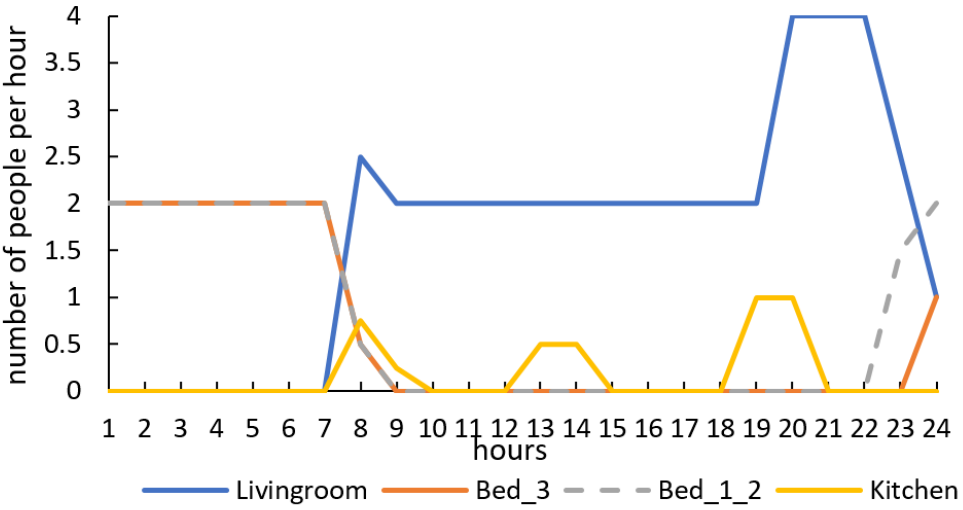

Figure 4: Occupancy rates of an average family

pants in the kitchen (170 W), passive occupants in the living room (125 W) and resting occupants in the bedrooms (80 W), according to EN 13799. A heat gain of 600 W was used in the kitchen during the cooking times (assuming an 80% efficiency of a 3,000 W stove/oven) and a constant 8 W/m^2 heat gain was assumed for all the house due to presence of different electrical equipment (value recommended by TRNSYS for a single family house based on SIA 2024).

Infiltrations were accounted as constant air changes per hour in each zone, depending on the number of windows and exterior doors. It was considered 0.75 air exchanges per hour (ACH/h) for each window and 1 ACH/h for each external door present in each zone. This led to a total average infiltration of 1.57 ACH/h for every flat, which coincides with values found by Navarrete [22] (1.27-1.52 ACH) and with those found by Diaz [23] (1.7 ACH). Besides the uncontrolled air infiltration, it was considered that windows are opened for 5 ACH/h in any zone that exceeded 23 °C.

The thermal demand of the building was calculated on an hourly basis using TRNSYS v18 according to Figure 5, with the building's characteristics modelled by Type 56. As the Chilean thermal regulation used in the simulation does not include any standard for floor insulation, the losses through the floor could be important and had to be modelled accurately. The under-slab ground was modelled using Type 49, which assigns a heat capacity and conductivity to the soil. This reduces the heat loss through the ground floor in winter, as the sub slab soil absorbs heat and increases its temperature with respect to the surrounding soil exposed to environmental conditions. As may be expected, it can take several years to reach a steady state as at

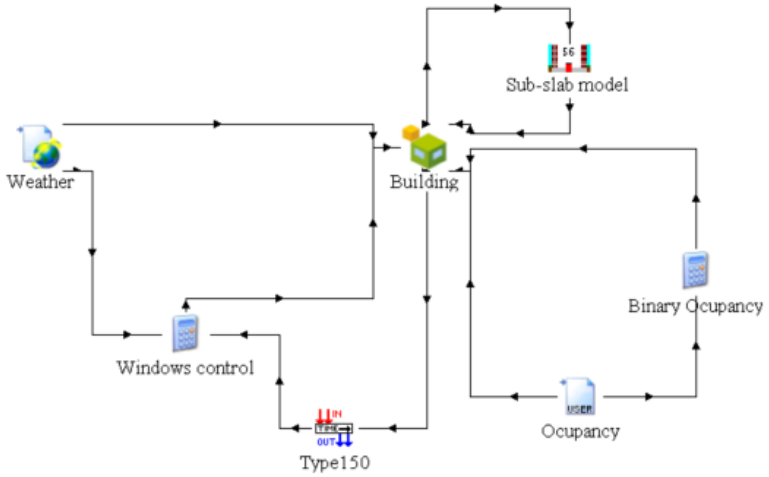

Figure 5: Diagram of simulation for calculating building's thermal demand in TRNSYS

the beginning the under slab soil is at the same conditions as the surrounding soil [24]. Therefore, the model was run for four years until the heat transfer and the temperature under the slab reached a steady periodic annual cycle. The weather data used was a typical meteorological year obtained from the solar explorer of the Chilean Ministry of Energy [25] which was compiled using data from 2004 to 2016 and was supplied to TRNSYS using a Type 15 weather data reader.

The system's performance was modelled for a system supplying heat to a development of 18 buildings such as those in Figure 3, totaling 144 flats. This configuration is referred as the Base case. In order to analyse the effect of heat demand density and scaling up of the system design, an alternative configuration with 1728 flats was also analysed. This configuration consists of a buildings' footprint eight times larger than the Base case and considered

Table 3: Difference in the two cases included in the analysis

	Base	Large
Total number of buildings	18	144
Flats per building	8	12
Total number of flats	144	1728
Floors per building	4	6

an extra duplex flat on top of those of the Base case. Hence, this second configuration, referred as the Large case, presents a 50% higher demand density and a 12 times higher total demand. This information is summarised in Table 3.

2.2. TRNSYS Simulation model

The system's operation was modelled using TRNSYS v18. (block 2 in Figure 2), extending an existing model developed by Renaldi & Friedrich [16] that replicates the system implemented in the Drake Landing Solar Community (DLSC) in Canada [17]. The main feature of this system is that it includes an underground long term storage system with a borehole technology (BTES) that allows for excess energy harvested during the summer to be stored for use in winter and can reach annual efficiencies of up to 60% [26]. The main parts and components of the system are schematically presented in Figure 6, while Figure 7 presents a to scale 3D view of a system configuration with 3,000 m^2 of collectors and 30,000 m^3 of LTS, along with a district of 144 flats, as the one used in the Base case. Figure 7 provides information about the relative dimensions of the different sub-systems.

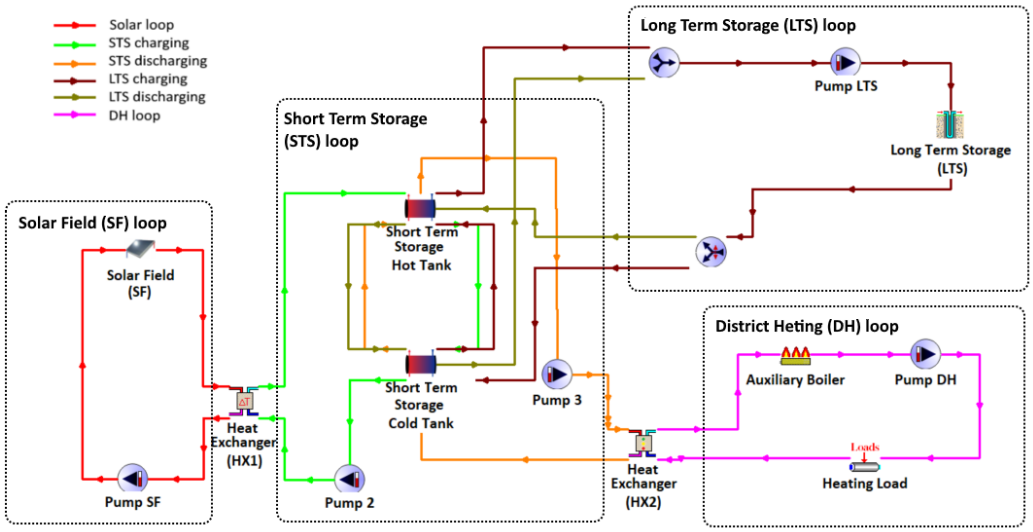

Figure 6: Main components of the TRNSYS simulation model

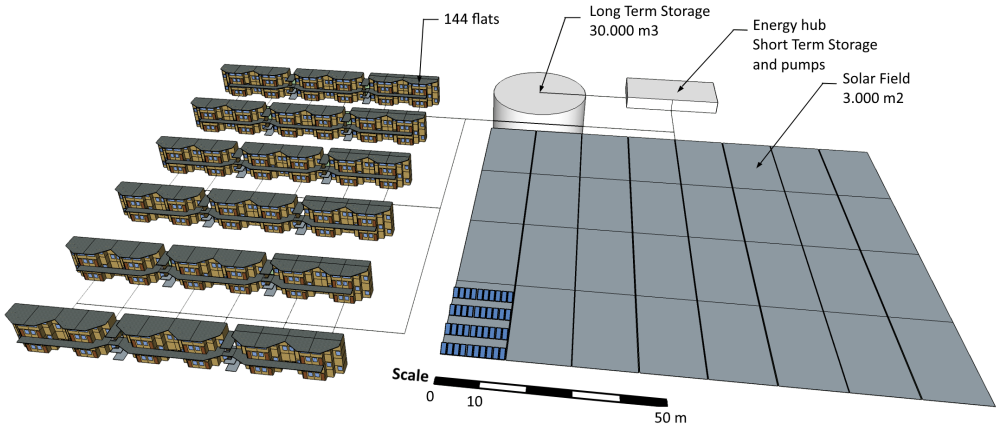

Figure 7: Scaled 3D model of a Base scenario system comprised of 144 flats, 3,000 m^2 collectors and 30,000 m^3 LTS

2.2.1. Solar field (SF) loop

The solar loop is harvesting solar energy in the form of heat. Its main component is the solar field, composed of parallel connected flat plate solar collectors with efficiency given by equation 1 and modelled with Type 1b.

$$\eta = 0.857 - 3.083\frac{T_{SF_{in}} - T_{ext}}{G} - 0.013\frac{(T_{SFin} - T_{ext})^2}{G} \quad (1)$$

All variable and parameters are defined in the nomenclature at the end of the manuscript. The solar field's working fluid is a glycol-water 30% mixture and is moved by a variable speed pump capable of pumping a maximum of 80 kg/h of fluid per square meter of solar field, which allows the actual maximum flow rate to change with the solar field's area. A heat exchanger with 80% effectiveness connects the solar loop with the short term storage.

2.2.2. Short term storage (STS)

The short term storage loop receives the heat from the solar loop and stores it in two stratified hot water tanks modelled with Type 534. One of these tanks stores the hot water coming from the solar loop or the long term storage during discharging at 70-90°C, while the cold water tank stores water coming from the district heating network or the long term storage during charging at 40-60°C. The STS acts as a hub that harvests the solar energy collected in the SF and decides whether to store the energy for a short term, deliver it to the district heating loop to fulfill the demand, or store or retrieve energy from the borehole long term storage. These decisions are made following the logic explained in 2.2.6.

2.2.3. Long term storage (LTS)

The long term storage subsystem consists of a borehole energy storage system (BTES) modelled by Type 557, which is based on the model developed by Hellström [27]. The pump of the LTS subsystem moves water from the centre to the perimeter of the storage during charging and from the perimeter to the centre during discharging at a constant 0.13 kg/s per each parallel string of boreholes. The geometry of the borehole storage is variable, depending on the total volume of the storage. However, certain rules were set, following the model of Renaldi and Friedrich [16]:

- The depth of the boreholes is equal to its diameter.
- The separation for boreholes in the same string is constant and equal to 2.25 m.
- The total number of boreholes grows proportional to the surface area of the LTS, starting from 144 boreholes for a surface area of 961 m^2 (corresponding to the original DLSC model developed by Renaldi and Friedrich [16]).

The soil thermal parameters used in the simulation are presented in Table 4 and were defined based on the description of the locations' geological conditions by Mella and Quiroz [28] for Temuco, de la Cruz et al. [29] for Coyhaique, and typical soil characteristics from Reuss [26].

2.2.4. District heating (DH) loop

The district heating system delivers hot water to the flats, represented in the model by a one node load. The load module (Type 682) fulfils the heating

Table 4: Soil characteristics in both locations

Location	Description	Thermal conductivity [W/K·m] [26]	Heat capacity [kJ/m^3] [26]
Temuco	Unconsolidated glacial gravel and sands deposits [28]	0.9	1,600
Coyhaique	Gravel and sand banks with silts subordinate [29]	1	

demand profile (calculated previously using Type 56) in each timestep by performing an energy balance on the hot water mass flow circulating in the DH and returning the water at a lower temperature, according to the energy balance. The water is moved by a variable flow pump and heated to a setpoint by means of a heat exchanger using hot water from the STS. A backup boiler (Type 659) provides the heat that is required to reach the setpoint if there is not enough energy available in the STS. The setpoint for the DH water is defined according to equation 2, the same used in the original Dake Landing project [30].

$$T_{DH_{setpoint}} = \begin{cases} 55°C & T_{ext} \leq -40°C \\ 0.48 \cdot T_{ext} + 35.8 & -40° < T_{ext} < -2.5°C \\ 37°C & T_{ext} > -2.5°C \end{cases} \quad (2)$$

A minimum heating temperature of 26°C is defined in the load module. This means that if the outlet temperature from the load module falls below 26°C, it is assumed that the load cannot be met by the DH.

2.2.5. Piping and pumps

The pipes were modeled as Type 31 TRNSYS elements. Although, the general piping layout followed the fixed design presented in Figure 7 The length of the pipes in the model is adjusted to follow the size of the SF and the number and configuration of the buildings in the district network. The pipe's diameter (D_{pipe}) is also adjusted to allow for a maximum flow velocity (v_{max}) of 1 m/s. These values are parameterised in TRNSYS, allowing for automatic adjustment of the dimensions for every configuration being evaluated.

The thermal loss coeficient of the pipes (I_{pipe}) was parameterised as a function of D_{pipe} using an approximation to the high quality pipes presented by Masatin et al. [31] according to equation 3

$$I_{pipe} = 0.1088 \cdot D_{pipe}^{-0.619} \quad W/m^2K \tag{3}$$

The rated power of each pump is calculated using v_{max} and the maximum head loss of each pipe using Darcy-Weisbach equation and Haaland's approximation for the Colebrook-White equation [32]. Approximated singular head losses, equipment head losses and the head due to buildings height were also included. This approach allows the model to adjust the "size" of the pumps for every configuration being evaluated. The instantaneous power demand of the pumps at each step of the simulation was assumed to change linearly with the flow rate.

2.2.6. Control strategy

The control strategies of the system are mainly the logic behind the operation of the pumps moving the working fluid and the decision whether to

charge or discharge the LTS. These are based on the work by Yang et al. [33] with slight modifications.

For the SF loop pump, a differential controller with hysteresis (Type 2b) is used. This controller turns the pump ON if the temperature difference between the fluid coming from the SF and the bottom of the cold STS (the coldest water in the STS) is higher than 10°C. It remains ON until that difference is less than 2°C or if the top of the hot STS (the hottest water in the STS) reaches 90°C. Additionally, during the ON status of the pump, it modulates its flowrate to keep a 10°C difference between the output and the input of the SF using a Type 22 controller. The pump connecting the SF loop with the STS modulates its flow to keep a 12°C temperature rise in the heat exchanger (HX1), while the pump connecting the STS with the DH loop modulates its flow to keep the DH water coming out the heat exchanger (HX2) at 37°C (according to equation 2). The DH pump is modulated to keep the return temperature in the system according to $T_{DH_{ret}}$ in equation 4, which is the approach used by Renaldi and Friedrich [16].

$$T_{DH_{ret}} = 0.9588 \cdot T_{DH_{sup}} - 4.79°C \tag{4}$$

As the approach of fixing the supply temperature of the district heating at the same value that a system designed for different demand and weather conditions may be sub-optimal, we also explore how the optimal configuration may change by using different supply and return temperatures ($T_{DH_{sup}}$ and $T_{DH_{ret}}$, respectively).

The charging of the LTS depends on the season of the year, so the controller was adapted from the model of Renaldi and Friedrich [16] to match

the seasons in the southern hemisphere. A diagram of the operation control logic under the different states of the LTS is presented in Figure 8. In summer the LTS starts being charged when the temperature difference between the top of the STS storage (hottest water in the STS) and the centre of the LTS (hottest zone of the borehole field) is above 10°C and it stops if that temperature difference falls below 3°C or if the average temperature in the LTS surpasses 90°C. In winter the charging is done only when the difference between the bottom of the STS storage (coldest water in the STS) and the DH water supply setpoint is above 10°C and the top of the STS storage is hotter than the centre of the LTS. The charging stops whenever the temperature difference between the bottom of the STS storage and the DH water supply setpoint falls below 2°C. The discharging process happens when the temperature difference between the centre of the LTS and the bottom of the STS is higher than 10°C and the top of the STS is below 55°C, and it stops when the aforementioned temperature difference falls below 3°C or the top of the STS drops under 55°C. A hysteresis effect was added to consider its previous step's state when deciding the next one. This avoids the charging process turning OFF when the temperature stays in between the "dead band". Table 5 summarises the logical equations behind the control strategy,

2.2.7. Performance indicators

The simulation set up in TRNSYS allows for multiple calculations of operation variables in every step and of performance indicators calculated during a year of operation or over the lifetime of the project. The main performance indicators of the operation of the system are:

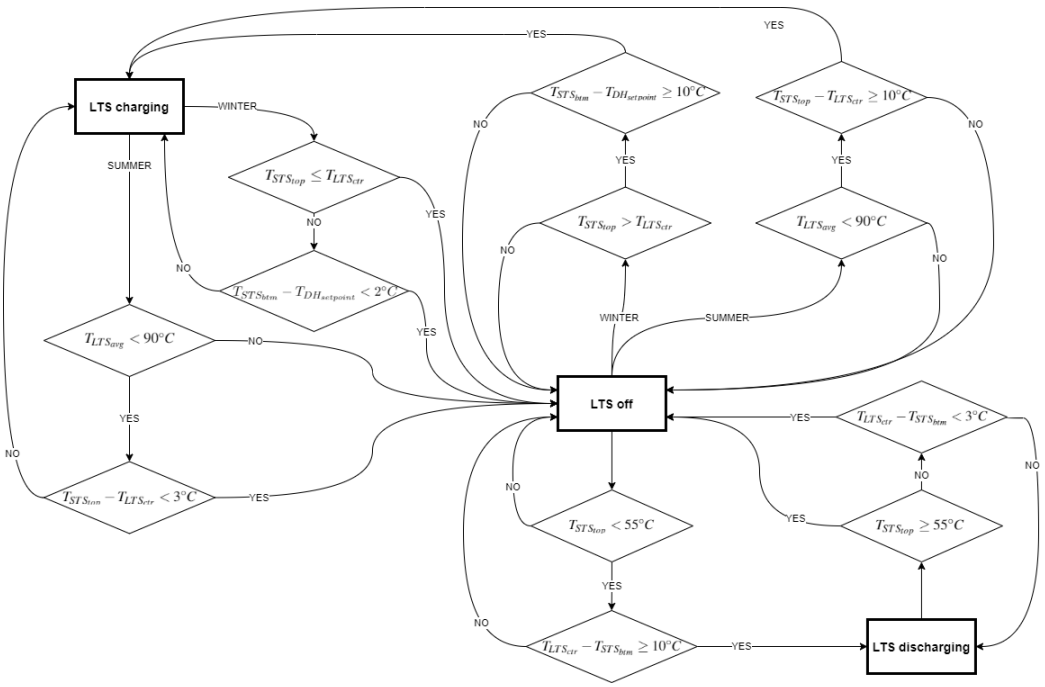

Figure 8: Logical operation diagram of the control of the LTS according to Yang et al. [33]

Table 5: Summary of the controller logic

System element	ON status conditions	OFF status conditions
SF loop pump	$T_{SF_{out}} - T_{STS_{btm}} \geq 10°C$	$T_{SF_{Pout}} - T_{STS_{btm}} < 2°C$ $\vee$ $T_{STS_{top}} \geq 90°C$
Pump connecting SF loop and STS	Flow modulated to keep $\Delta T_{HX1_{STS}} = 12°C$	
Pump connecting STS and DH	Flow modulated to keep $\Delta T_{HX2_{DH}} = T_{DH_{setpoint}}$	
DH pump	Flow modulated to keep condition in equation 4	
LTS charge summer	$T_{STS_{top}} - T_{LTS_{ctr}} \geq 10°C$ $\wedge$ $T_{LTS_{avg}} \leq 90°C$	$T_{STS_{top}} - T_{LTS_{ctr}} < 3°C$ $\vee$ $T_{LTS_{avg}} > 90°C$
LTS charge winter	$T_{STS_{btm}} - T_{DH_{setpoint}} \geq 10°C$ $\wedge$ $T_{STS_{top}} > T_{LTS_{ctr}}$	$T_{STS_{btm}} - T_{DH_{setpoint}} < 2°C$ $\vee$ $T_{STS_{top}} \leq T_{LTS_{ctr}}$
LTS discharge	$T_{LTS_{ctr}} - T_{STS_{btm}} \geq 10°C$ $\wedge$ $T_{STS_{top}} < 55°C$	$T_{LTS_{ctr}} - T_{STS_{btm}} < 3°C$ $\vee$ $T_{STS_{top}} \geq 55°C$

- Solar fraction (SFr): is the fraction of the total load that is fulfilled with solar energy, which corresponds to the energy exchanged in the heat exchanger connecting the STS and the DH (HX2), divided by the total energy used to fulfil the load, which corresponds to the solar energy delivered to the DH plus the energy supplied by the boiler, according to equation 5.

- Solar system efficiency (η_{Ssys}): is the performance of the system using the solar energy collected. It is calculated as the ratio between the energy delivered to the DH and the energy collected in the SF, according to equation 6.

- LTS efficiency (η_{LTS}): is the efficiency of the LTS in storing the energy. It is calculated as the ratio between the energy discharged from the LTS and the energy charged into the LTS, according to equation 7.

$$SFr = \frac{\int \dot{Q}_{HX2}}{\int \dot{Q}_{HX2} + \int \dot{Q}_{boiler}} \tag{5}$$

$$\eta_{Ssys} = \frac{\int \dot{Q}_{HX2}}{\int \dot{Q}_{SF}} \tag{6}$$

$$\eta_{LTS} = \frac{\int \dot{Q}_{LTS_{disch}}}{\int \dot{Q}_{LTS_{charge}}} \tag{7}$$

2.2.8. Economic indicators

The economic indicator used to evaluate and compare the performance of the system is the levelized cost of energy (LCOE), which takes into consideration the initial investment and the variable and fixed costs of operating

Table 6: Unitary costs of energy and annual cost of operation and maintenance

	Cost	Unit	Ref.
Operation & Maintenance ($C_{O\&M}$)	$0.0075 \cdot C_{inv}$	€/a	[36]
Natural Gas Temuco (C_{fuel})	0.05	€/kWh	[37]
Diesel Coyhaique (C_{fuel})	0.06	€/kWh	[38]
Electricity (C_{elec})	0.1	€/kWh	[39, 40]
Carbon tax	0	€/kgCO_2	

the system to calculate an annualised cost of energy production during the lifetime of the project according to equation 8 assuming a discount rate $r = 0.05$ and a lifetime n=25 years. This discount rate is slightly lower than the 0.06 recommended in Chile for public building projects [34] and a close to those proposed for the long term evaluation of public projects by Edwards [35].

$$LCOE = \frac{C_{inv} + \sum_i^n \frac{C_{O\&M}+C_{fuel}+C_{elec}}{(1+r)^i}}{\sum_i^n \frac{Q_{load}}{(1+r)^i}} \tag{8}$$

The different annual costs are calculated in TRNSYS using the values in Table 6, while the investment costs are calculated using the unitary costs in Table 7.

2.2.9. Emission indicators

As emission indicator ,the specific emission per unit of energy output (SE) is defined according to equation 9. This equation considers the emission coming from the fuel burned by the auxiliary boiler as well as the indirect emission from the electricity consumed by the pumps and is divided by the

Table 7: Unitary investment costs of equipment

		Cost	Unit	Ref.
Solar field (C_{SF}) (including pipes)		$3.8 \cdot 10^{-8} \cdot SF_A^2 - 3.9 \cdot 10^{-3} \cdot SF_A + 271$	€/m^2	[12]
Short term storage (C_{STS})		$43 \cdot STS_{vol}^{-0.467} + 250$	€/m^3	[36]
Long term storage (C_{LTS})		$2,600 \cdot LTS_{vol}^{-0.47}$	€/m^3	[41]
Buried pipes (C_{pipes})		$4334 \cdot D_{pipe}^2 + 4011.7 \cdot D_{pipe} + 198.7$	€/m	* [42]
Boiler (C_{boiler})		$24.8 \cdot \bar{Q}_{boiler} + 31,850$	€	[43]
Indoor system (C_{HDS})		$12560 \cdot LMTD^{-1} + 522$	€/flat	**
Pumps (C_{pumps})	single speed	120	€/kW	***
	variable speed	240		

* Insulated pipes, considers feed and return pipe in the same trench

** Considering a linear relation with a standard 75°C supply temperature system at 700 €/flat and a 37°C supply temperature system (DLSC standard) at 1500 €/flat. Internal temperature (T_{int}) assumed 21°C for $LMTD$ calculation. $LMTD = \frac{T_{DH_{sup}} - T_{DH_{ret}}}{\ln \frac{T_{DH_{sup}} - T_{DH_{int}}}{T_{DH_{ret}} - T_{DH_{int}}}}$

*** Standard values used in engineering projects

Table 8: Emission factors of the fuel and electric systems considered in the model

	Emission Factor	Unit	Ref.
Natural Gas	0.204		[45]
Electric grid Temuco	0.25	[kgCO_2/kWh]	[44]
Electric grid Coyhaique	0.25		*

* In 2016, the emission factor of this system was 0.33 kgCO_2/kWh [46] with a reduction trend expected.

total energy supplied by the system.

$$SE = \frac{EF_{grid} \cdot \int \dot{Q}_{pumps} + EF_{fuel} \cdot \int \dot{Q}_{fuel}}{\int \dot{Q}_{load}} \tag{9}$$

The emission factors of the fuels and the electric grid are presented in Table 8. The electric grid emission factor for Temuco for 2025 was used, according to scenario "C" and a dry hydrology in the Chilean "long term energy plan" [44]. In the case of Coyhaique, there is no up to date information nor projections of the emission factor of the isolated Aysen system (where Coyhaique is connected). Therefore, the same value as for Temuco was used.

2.2.10. Simulation parameters

As the optimisation process requires thousands of runs of the simulation model, a balance between simulation run speed and accuracy needed to be reached. Considering this, a 10 minutes time step was chosen, as it allows to run a one year simulation in around 1 minute and is short enough so Type 31 plug flow pipes model does not have convergence errors which occur when the residence time inside a pipe element is smaller than the timestep. The

simulation of a complete year of operation is important in the context of a LTS economic operation analysis, as it allows to completely integrate the time domain through a continuous operation. This contrasts with other approaches, that use aggregated time periods to represent representative weeks or days of the year, which allows a faster simulation, but fails to address the time coupling of the LTS state of charge.

Due to the slow heating of the soil from its normal temperature, there is a four to six years period to get the LTS to a steady state operation. In order to reduce the simulation time, a preliminary analysis was performed on the average LTS temperature at the end of a five years run with different system configurations. A parametrisation of this temperature as a function of the main parameters (SF_A and LTS_{vol}) allowed to define a function that approximates the average temperature conditions in the LTS ($T_{LTS_{avg}}$) at the beginning of a year in a steady state operation. This allowed to start the simulation from a condition akin to that after five years of operation. Eventually, it was found that running the simulation for two years got results with less than 5% difference in the performance of economic and emission indicators if compared with a full five years run. The first of these two years was used to smooth out any differences in LTS temperature after applying the parametric approximation for $T_{LTS_{avg}}$, while the second year's result were considered for the optimisation.

2.3. Optimisation model

The last step of the method used in this work, shown in block 3 in Figure 2, is a routine that performs the optimisation by running several systems configurations and chooses those that minimise the cost and the emissions.

After every generation a new Pareto front that approximates closer to the true optimal solution is generated. An optimisation routine was implemented in Python using a genetic algorithm provided by DEAP and it was linked to the TRNSYS simulation model, reading TRNSYS's outputs and modifying TRNSYS deck file (inputs).

2.3.1. Objective function

The objective of this optimisation is to determine system configurations that are both cheap and that produce low emissions. Hence, $LCOE$ and SE (equations 8 and 9) were defined as the objective functions to be minimised, as it is expressed in equation 10. x^{min} and x^{max} are adjusted according to the case that is being optimised. These adjustments do not affect the final result, but allow for a quicker convergence of the Pareto front. As $LCOE$ and SE are mutually opposing, a set of optimal configurations that trade between cost and emissions is expected.

$$Min \begin{cases} LCOE(x_i) \\ \qquad\qquad i \in \{1, ..., n\} \\ SE(x_i) \end{cases} \tag{10}$$

$$0 < x_i^{min} < x_i < x_i^{max},$$

with x_i^{min} and x_i^{max} adjusted according to the system being assessed

Next subsection identifies the variables (x_i) used in the optimisation problem.

2.3.2. Optimisation Variables

In a preliminary analysis the equipment that is more influential in the performance of the system was assessed, and it was found that the most important variables in the system configurations were the area of the solar collectors field (SF_A), volume of long term storage (LTS_{vol}) and volume of short term storage (STS_{vol}). Therefore, these were included as the main optimisation variables in the model. Changing the size of these values has an impact in the investment cost and produces an effect on the performance of the system, as well as in its running cost. A combination of values for these three optimisation variables defines a system configuration. The run of the simulation with this configuration returns the evaluation of the objective functions, which later could be assessed for the optimality of that configuration. As a fourth variable, the tilt angle of the solar collectors (θ) was included in the optimisation. Although this variable has a comparatively lower influence in the cost and emission assessment, its analysis is interesting as it is a way to produce a slight improvement in the system's performance without any additional cost and, as it will be discussed in 3.3 the choice of an optimal θ is not straightforward. Additionally, as mentioned in 2.2.6, the effect of considering different $T_{DH_{sup}}$ and $T_{DH_{ret}}$ in the district heating network was analysed

2.3.3. Optimisation routine

The optimisation is performed by DEAP [47] using the eaSimple algorithm for evolving the population and NSGA II for sorting the best individuals. The crossover was performed by two points crossover and the mutation by polynomial bounded mutation [48]. The main parameters of the optimi-

sation process are presented in Table 9.

As a high mutation probability tends to lead towards a random search of the optimum, while a low probability tends to miss large areas of the solution space and risks missing the global optimum [49], the mutation probability (P_{mut}) was modified in each iteration (i) with a Gompertz function according to equation 11.

$$P_{mut_i} = P_{mut_0} - (P_{mut_0} - P_{mut_N}) \cdot e^{-b \cdot e^{-c \cdot i}} \tag{11}$$

The parameters used for this equation were: P_{mut_0}=0.7, P_{mut_N}=0.03, b=5, c=0.08 and N =10, which produces a curve that allows for some initial exploration of the solution space and a better converging towards the end of the optimisation.

3. Results and discussion

This section presents the main results of the study, starting with the calculation of the thermal loads in both locations, following with the analysis of the optimisation results for the different locations and configurations and an estimation of the sensitivities of the results to the main economic assumptions.

3.1. Heating demand analysis

The results from the thermal load simulation showed that the thermal consumption of the ground level flats is on average 2-4% higher than those in the upper level. This is mostly due to the absence of insulation between the floor and the slab. The results also showed a slightly higher demand during

Table 9: Main parameters of the genetic algorithm optimisation

Parameter	Value	Definition
Number of generations (N)	120	Number of iterations of the algorithm
Population	80	Initial number of individuals and number of individuals that survive after each iteration
Crossover prob.	0.7	Probability of an individual exchanging genes with other
Individual mutation prob.	Eq. 11	Probability of an individual being subjected to a mutating process
Gene mutation prob. in a mutating individual	0.3	Probability of an individual gene mutating in each mutating individual

Table 10: Results of annual thermal load calculations in both locations.
GF stands for Ground Floor and UF for Upper Floor

	GF Ext.	UF Ext.	GF Int.	UF Int.	Average flat	Unit
Temuco	126.2	121.1	112.1	106.4	116.4	[kWh/m^2·a]
Coyhaique	225.2	221.6	202.4	197.1	211.6	

the first year of operation due to the initial ground temperature under the slab. However, this difference was below 1% and the yearly average under slab temperature stabilized after two years of operation. Table 10 shows the annual thermal loads of the flats depending on their location in the block for the two cities. "Exterior" flats correspond to those at edges of the block with three of their sides exposed to the environment, while "interior" flats correspond to flats with two of their sides exposed to the environment.

These values agree with those defined as base values for the Chilean thermal rating system that sets a base cases for flats at 108 and 220 kWh/m^2·a for Temuco and Coyhaique respectively [50]. They also match closely values reported by Bustamante et al. [51] that uses 125 kWh/m^2·a for one floor continuous façade social housing in Temuco and 252 kWh/m^2·a for the same configuration in Punta Arenas, a city with 13% higher annual degree days heating requirements compared to Coyhaique. Figure 9 presents the monthly energy load comparison between an average flat in both locations.

Considering these demands and the layout of the system the main demand parameters of the systems in both locations are presented in Table 11. In general, the literature mentions a broad band around 1.5 MWh/m·a of lin-

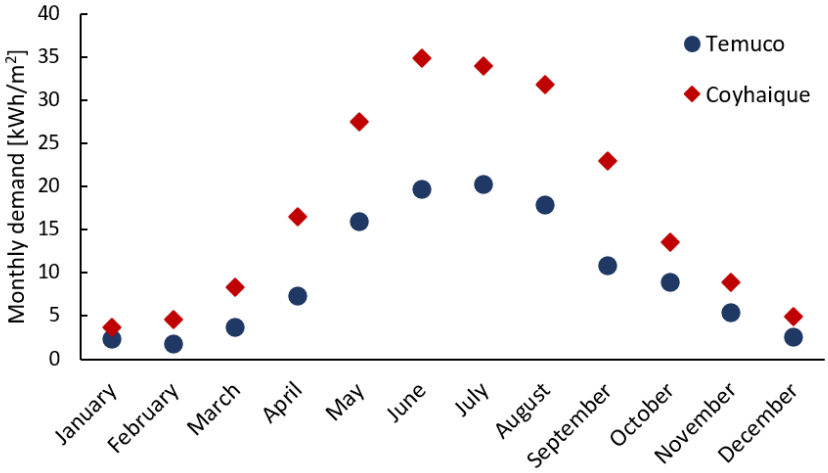

Figure 9: Monthly thermal demand for an average flat in both locations

ear energy density as a threshold for economic viability for new-constructed district heating networks [52, 53] and some works use higher values such as 2.5 MWh/m·a [54] or even 4 MWh/m·a [55]. The Chilean guide for district heating project development recommends densities above 70 kWh/m^2·a for potentially successful projects [56]. A system with lower linear energy density has relatively higher thermal losses and higher cost in piping which makes it economically less competitive. Considering this, it is expected that the Large system would have a better performance due to higher energy densities.

3.2. Pareto front analysis

The main outcomes of the optimisation process are the Pareto fronts. These curves present the set of non-dominated solutions that minimise the $LCOE$ and the SE. The TRNSYS simulation presented convergence problems for LTS volumes around 3,000 m^3 and below in Type 557. This meant that two optimisations were run for the same location: one with LTS and

Table 11: Main demand metrics of the different locations and systems

	Temuco		Coyhaique		Unit
	Base	Large	Base	Large	
Total annual demand	854	10,248	1,554	18,648	[MWh]
Peak demand	706	8,472	855	10,260	[kW]
Annual load factor	0.14		0.21		[-]
Linear demand density	1.2	1.9	2.5	3.5	[MWh/m·a]
Area energy density	76	114	139	208	[kWh/m^2·a]

volumes of 3,000 m^3 and above, and a second without LTS where the LTS loop, including Type 557, was removed.

The optimisation presents a good convergence of the Pareto front. Within the first 10 generations the Pareto front converges close to its final value and in further generations it populates and diversifies the set of solutions, as it was intended by using equation 11 for the definition of the optimisation routine parameters. This can be graphically appreciated in Figure 10, which presents the evolution of a number of generations for the optimisation of the Base case in Coyhaique.

Figure 11 presents the Pareto front resulting from these optimisations for the location in the cities of Temuco and Coyhaique for the Base case, while Figure 14 presents the results for the Large case. Both cases' configurations are described in Table 3 and their demand features in Table 11. The final system's Pareto front curve can be approximated by considering the non dominated points of the addition of both curves. Other than the objective functions, Figures 11 and 14 provide information of the SFr in the color

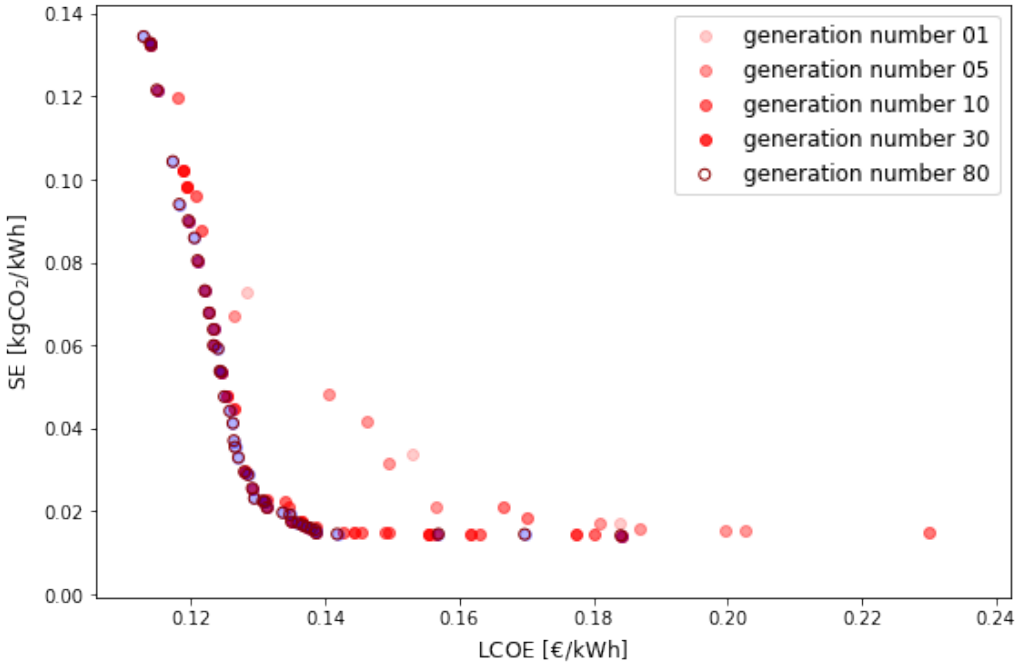

Figure 10: Pareto front evolution during an 80 generation run for the Base case in the city of Coyhaique with an initial population of 80 individuals

scale and η_{LTS} in the size of the point markers.

Figure 12 presents the evolution of the optimisation variables and of the performance indicators for the system configurations in the Pareto front in Coyhaique and Temuco for the Base case with LTS, while Figure 15 presents the evolution of the optimisation variables and of the performance indicators for the system configurations in the Pareto front for the Large case in both cities. These figures present the non dominated points considering the curves with and without LTS.

Figures 13 and 16 present the net cost structure of a subset of configurations in the Pareto front in both locations for the Base and Large case respectively. The investment costs are presented in solid colours and are calculated using the information in Table 7, while annual costs are presented in pattern colours and are calculated using the information in Table 6 and discount rate $r = 0.05$ and lifetime n=25 years to bring the annual costs to present value. Each configuration's SE is plotted on the right axis as a reference and the configurations highlighted in Figure 11 are outlined.

The most evident result from Figure 11 is that the system in Coyhaique reaches costs around 0.4 €/kWh lower than Temuco. This is mostly due to the better utilisation of the invested infrastructure in Coyhaique, as it operates longer time closer to its peak capacity, achieving a higher load factor, as shown in Table 11. This can be corroborated with Figure 13, that shows that the total costs for the system in Coyhaique are between 35 and 60% higher, while the annual energy demand is 82% higher.

As a comparison, two conventional heating options are presented in Figures 11 and 14. A "fossil district network" that represents a district heating

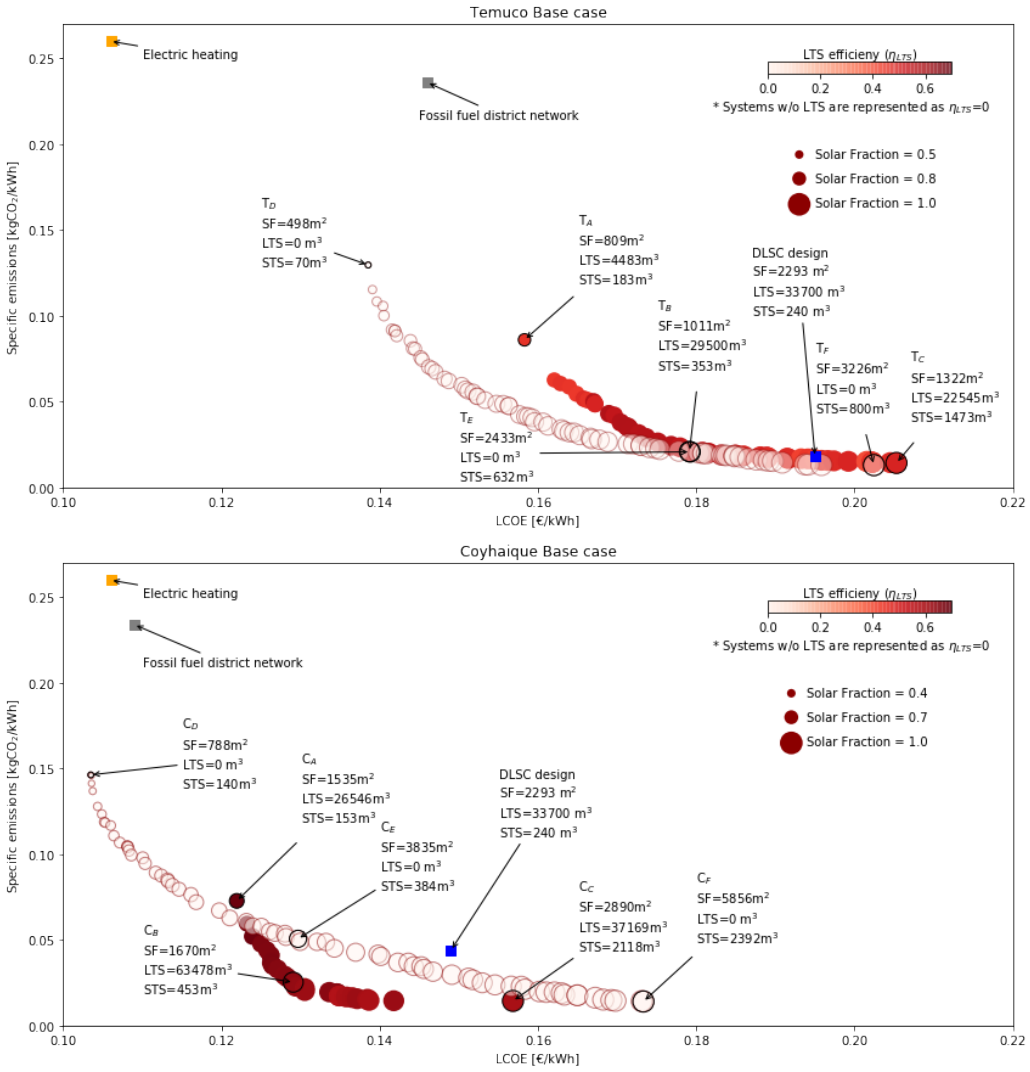

Figure 11: Pareto fronts for the Base system with and without LTS (the later represented as white circles with 0% LTS efficiency)

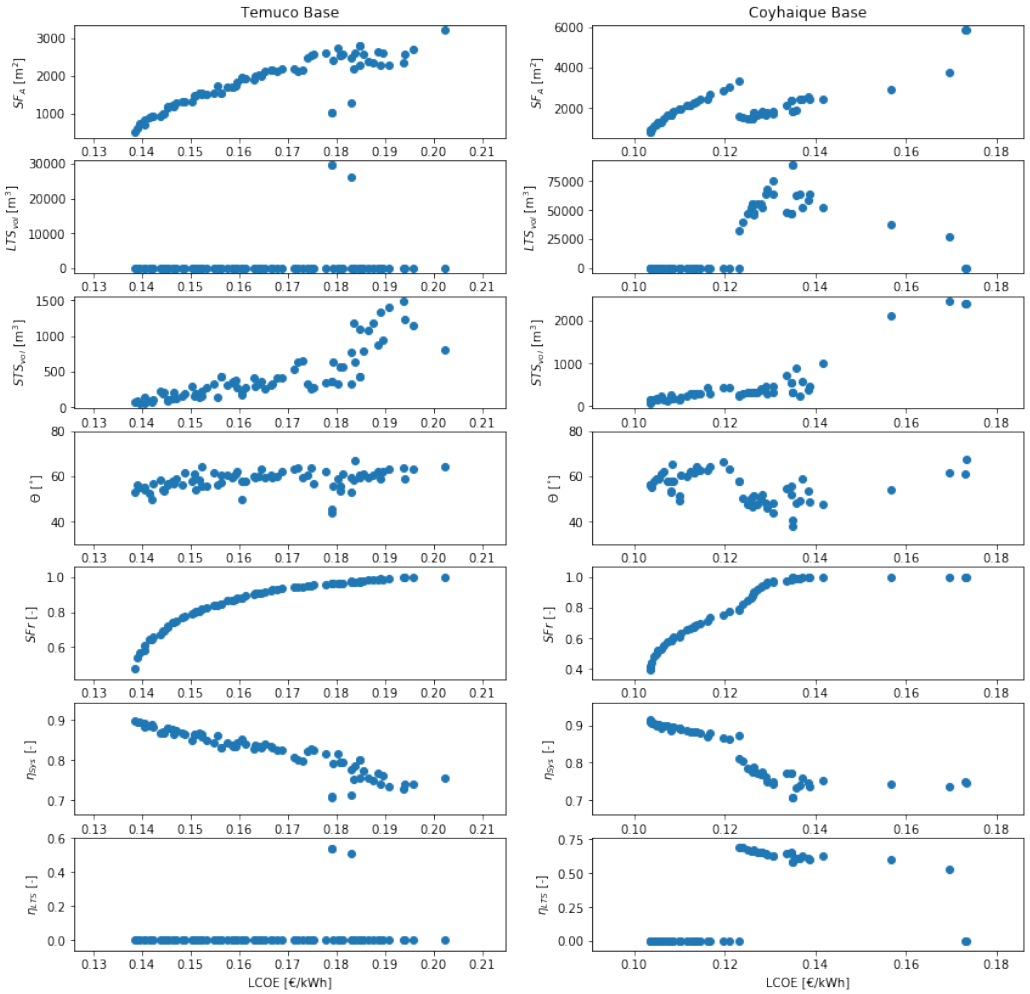

Figure 12: Values of optimisation variables and performance indicators for the systems in the Pareto front for the Base case in Temuco (left) and Coyhaique (right)

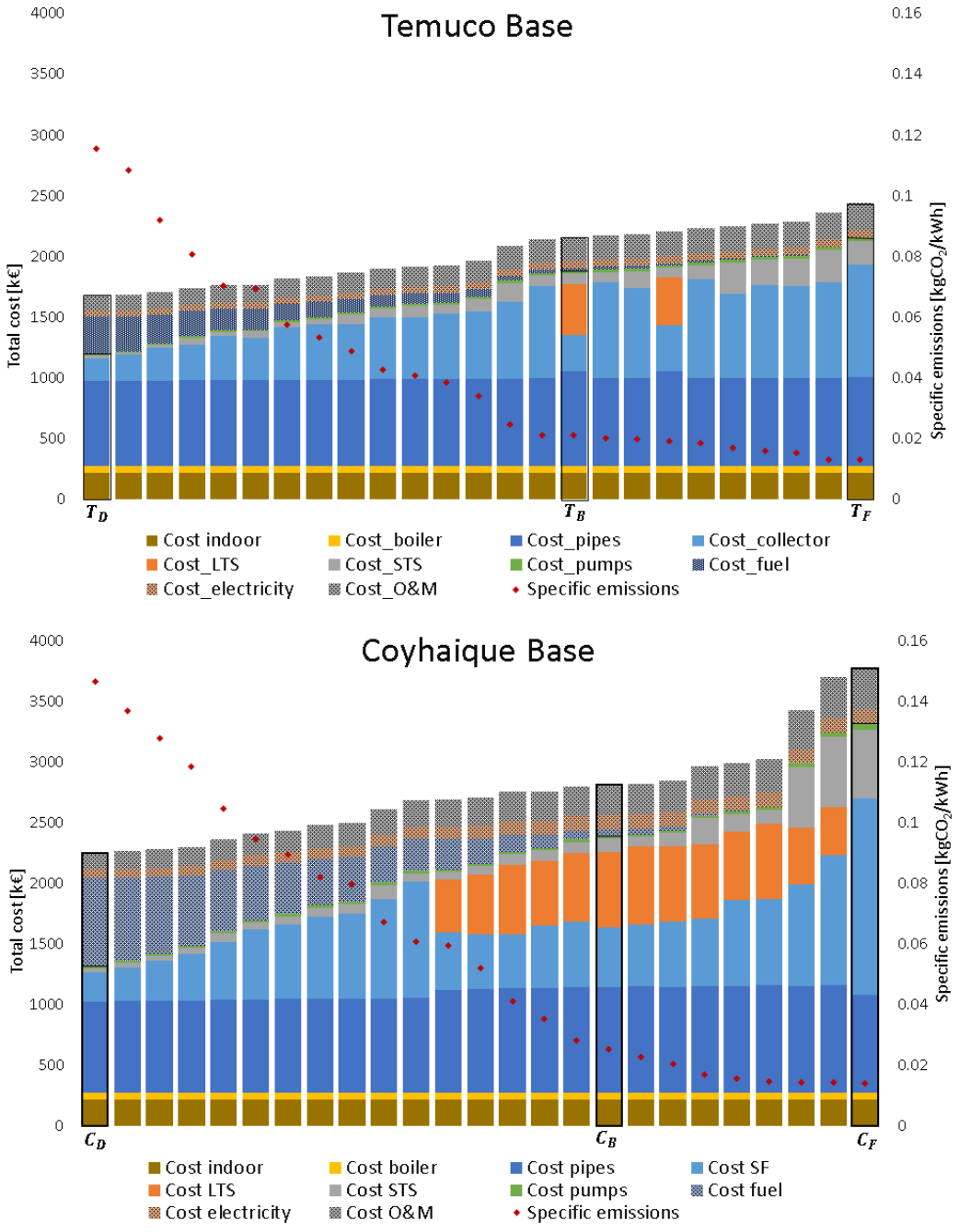

Figure 13: Cost structure of all the system configurations in the resulting Pareto front for the Base case in both locations

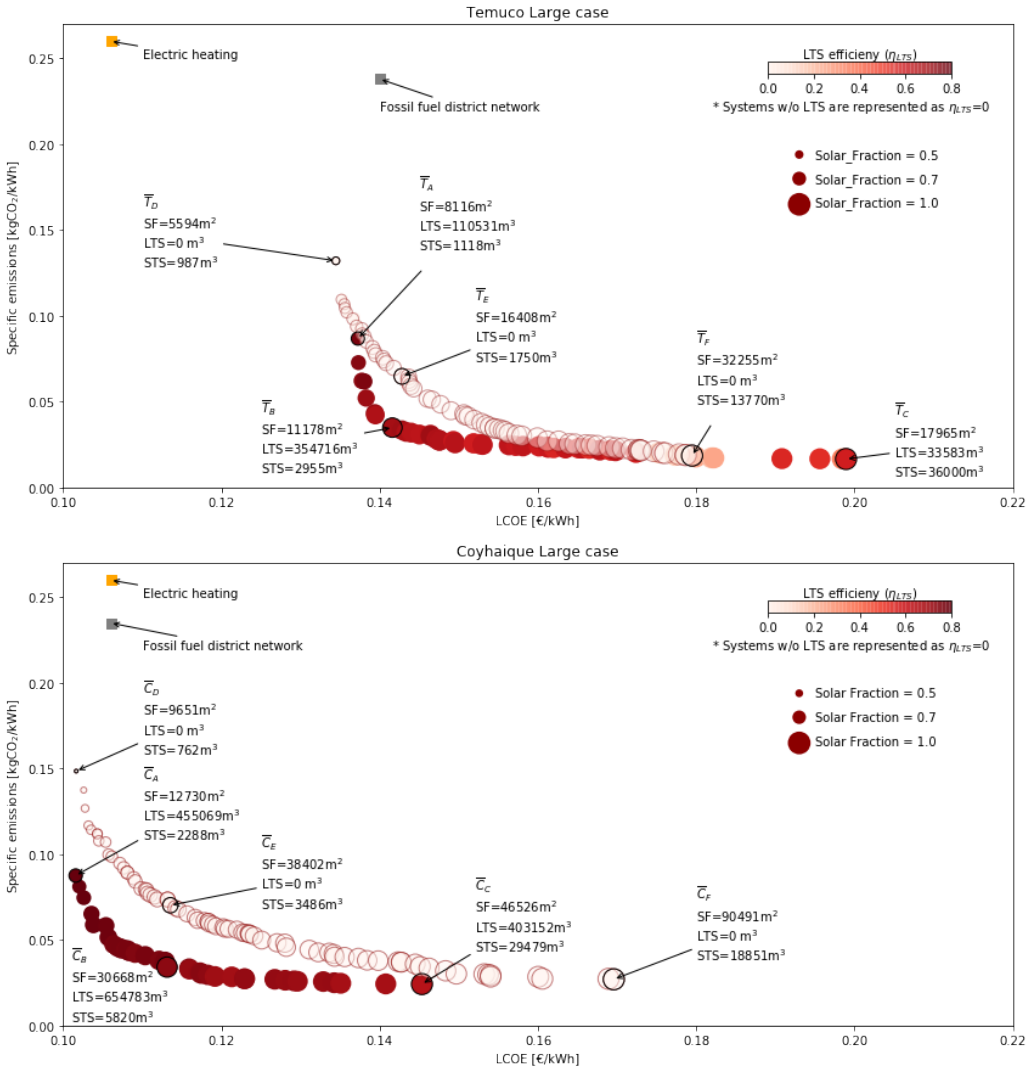

Figure 14: Pareto fronts for the Large system with and without LTS (the later represented as white circles with 0% LTS efficiency)

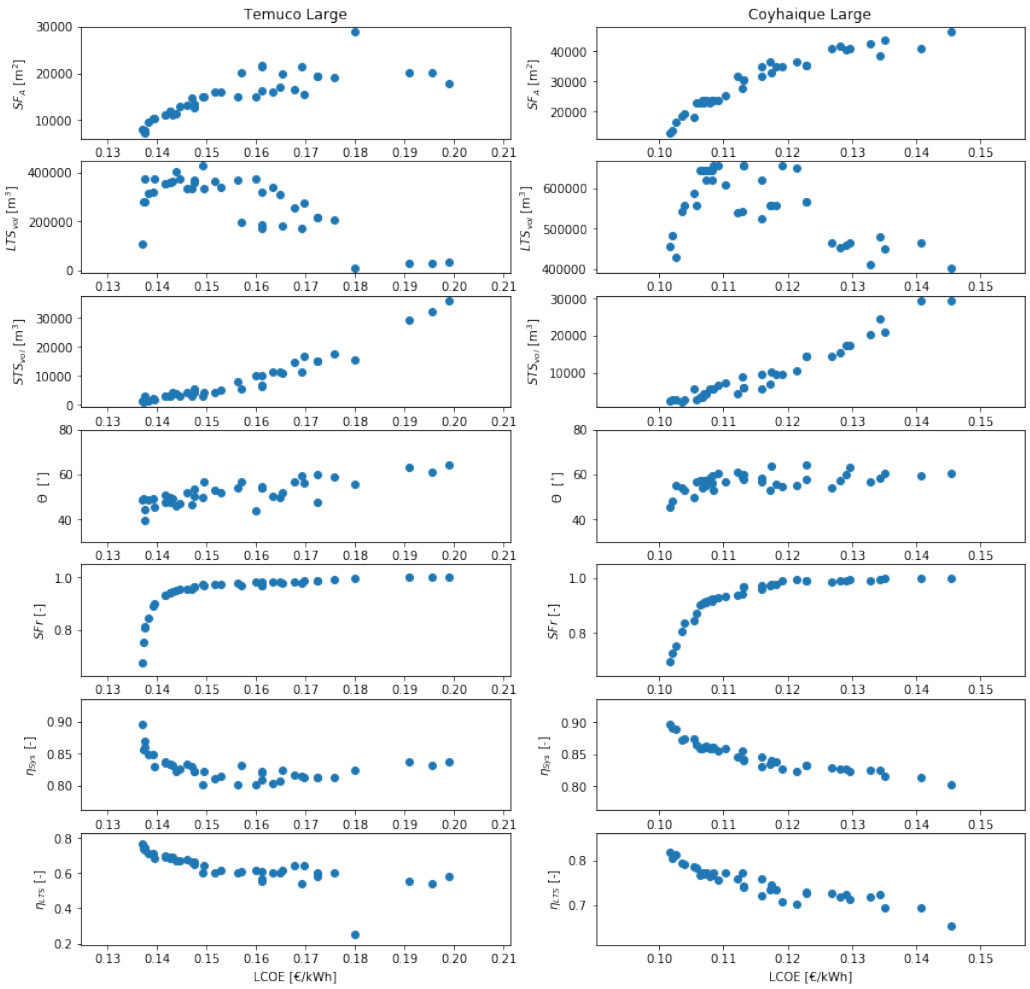

Figure 15: Values of optimisation variables and performance indicators for the systems in the Pareto front for the Large case in Temuco (left) and Coyhaique (right)

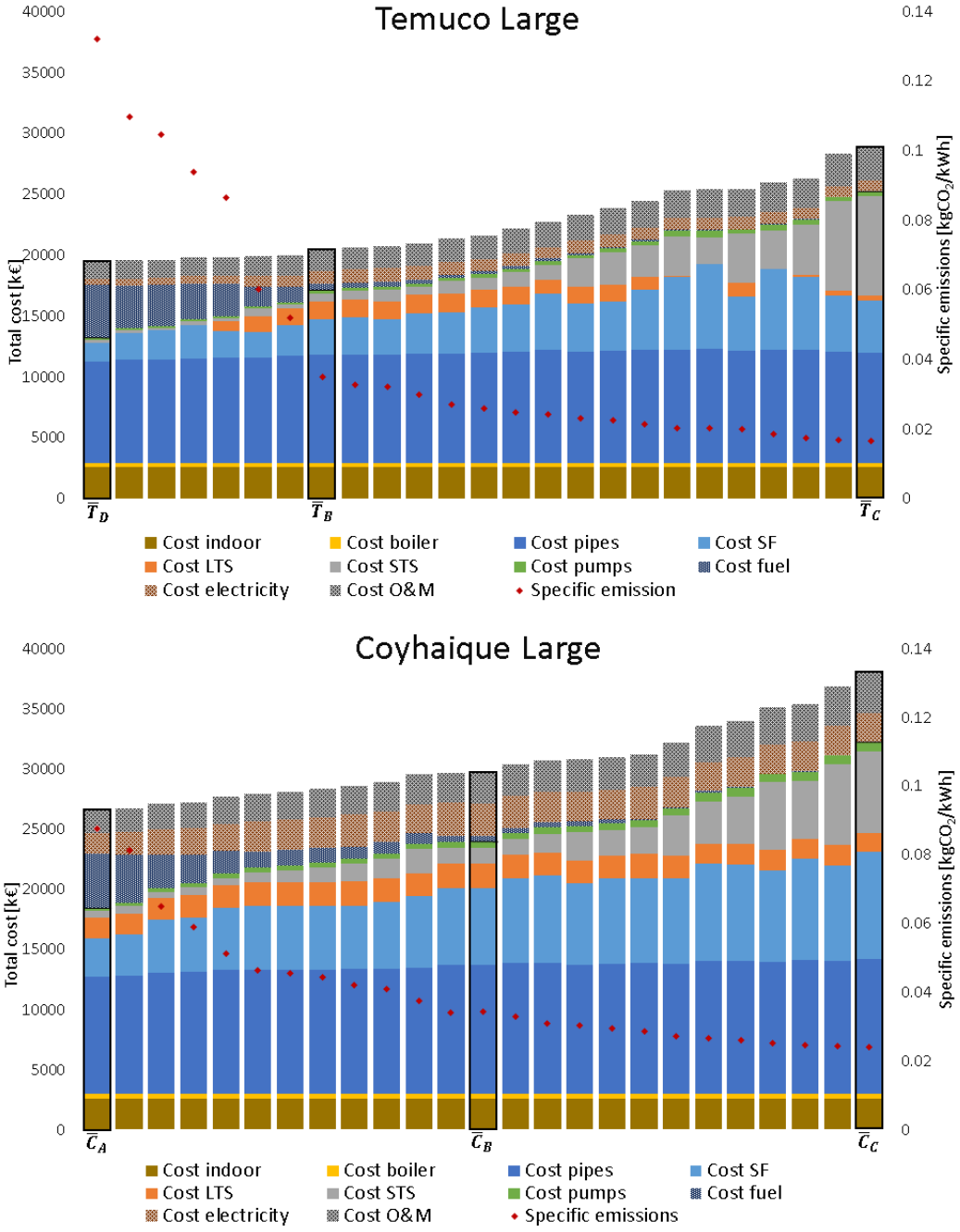

Figure 16: Cost structure of all the system configurations in the resulting Pareto front for the Large case in both locations

system that provides heat from a gas boiler and "electric heaters" represents local electric resisitive heaters located in the flats. It can be seen that in both cities solar systems can compete in cost with fossil fuel alternatives. However, only in Coyhaique the solar alternatives can compete with electric heaters in the Base case. Most notably, configurations such as that represented by point C_B can decrease the SE by around 90% with respect to conventional alternatives by increasing the costs by less than 20%.

For the city of Temuco, Figure 11 shows that the configurations without LTS dominate those with LTS. This means that it is cheaper to have a larger SF and eventually curtail some solar energy than invest in a LTS and store energy, as the operation of the LTS yields efficiencies around 40-45%. For systems with LTS higher than 20,000 m^3 and SF around 1,200 m^2 there is an increase in the efficiency of the LTS to more than 50% and the $LCOE$ of the systems with LTS becomes comparable to those without LTS. This is evident for system configuration T_E and can be seen in Figure 12, where some points with LTS > 0 appear in the plots, producing a subsequent drop in SF_A and in η_{Ssys}. This also is evident in Figure 13, where for configuration T_B the LTS replaces part of the SF. However, in most of the cases for the Base case in the city of Temuco it is most cost efficient not to consider a LTS.

It is interesting to note that in Figure 11, configurations T_C and T_F have already reached $SFr = 1$, which implies that the fuel consumption has reached zero and the emissions cannot be reduced more, as increasing the storage or the solar field area would mean higher electricity consumption associated to pumping, thus increasing the SE. This behaviour is common to all the cases analysed so the Pareto fronts do not converge to a SE value

and for larger $LCOE$ the emissions start to increase.

In the case of Coyhaique, similarly to Temuco, the Base case without LTS dominates the case with LTS for smaller system configurations. However, the inclusion of LTS in this location leads to further SE reductions. This is probably related to the LTS being used more and reaching η_{LTS} close to 70%. In particular, for a similar $LCOE$, configuration C_B reduces emissions in more than 50% in comparison with configuration C_E by reducing SF to 50% and adding a LTS of almost 65,000 m^3.

From Figure 12 in Coyhaique, it can be noticed that the optimal tilt angle (θ) of the solar collectors shows variation along the Pareto front. This finding contrasts to what could be expected, as usually optimal annual yield tilt angles tend to be related to the latitude of the location, and the nature of this variation is discussed in depth in section 3.3.

Similarly to the results in Figure 11, Figure 14 shows that the cost of the Large system in Coyhaique is around 0.04 €/kWh lower than in Temuco. On the other hand, the minimum SE achieved at $SFr = 1$ is higher in the Large case in comparison to the Base case. This is a direct effect of the systems in the Large case having to use comparatively more energy for pumping, due to longer pumping networks in the DH network, SF and LTS. This can be seen in Figures 13 and 16, where the fraction of the total cost represented by the use of electricity increases from around 3-4% in the Base case to around 6-9% in the Large case.

Furthermore, the solar systems are again comparable in cost with conventional alternatives achieving emission reductions by more than 80% in comparison to conventional alternatives by increasing the cost by only 2%,

as shown by configuration $\overline{T}_B$ in Figure 14. In addition, the $LCOE$ in both cities decreased by 0.15-0.20 €/kWh in comparison with the Base case. This is also an effect of a larger system, but even more, a product of the higher energy density considered for the Large case, highlighting the importance of dense energy demands areas for the competitiveness of district network systems. Another difference with respect to the Base case, is that Figure 14 shows that the configurations with LTS dominate the curve without LTS for both cities, meaning that it could be cost efficient implementing LTS for the Large case. In this configurations very large LTS systems of more than 600,000 m^3 reach efficiencies close to 80%.

Figures 13 and 16 clearly show that the piping of the district network is one of the dominant costs of the systems. However, its relative importance decreases for systems with larger SFr, as investments in SF and in storage start to dominate. From these figures, it is also interesting to highlight that the increase in size of LTS has no noticeable effect on the size of STS, but it decreases notable the size of the SF. This is due to the slow thermal inertia of the BTES technology which does not allow it to provide the quick response operating service provided by the STS tanks, but increases the SFr by supplementing the operation of the SF in periods with lower irradiance and higher heating demand.

The $LCOE$ of the systems for both locations and cases analysed ranged between 0.1 and 0.2 €/kWh, depending on the systems configuration. This is comparable with other values found in the literature for similar systems. Schmidt et al. [57] calculated values between 0.17 and 0.42 €/kWh for systems with different long term storage technologies in central Geramany. Re-

naldi and Friedrich [16] estimated values of $LOCE$ of 0.20 and 0.27 €/kWh for locations in Scotland and England for a similar system composition, but without performing an optimisation. Hsieh et al. [58] performed an analysis on a system in Switzerland, achieving close to 0.4 €/kWh for a configuration with centralised long term storage and heat generation, but the system in their case was much smaller, with energy demands around 5 to 10 times lower than those considered in this study. Mauthner and Herkel [59] analysed systems in central European locations and BTES technology for the long term storage and reached $LCOE$ values between 0.10 and 0.17 €/kWh.

Even though the cost of the solar district heating networks analysed in this study can be competitive with some conventional alternatives, they are not currently competitive with burning firewood (the main source of domestic heating in the cities of southern Chile), which has an $LCOE$ between 0.025 and 0.035 €/kWh [60]. In order to compete with this technology, economic incentives that account for the negative externalities caused by the PM2.5 pollution should be put in place. Most of these externalities are related to health issues and subsequent increased load in the health system and increase in sick days. For instance, if considering social cost of PM2.5 emissions of 15.000 US$/tPM2.5 [61] and an emission factor of 0.5 g$PM_{2.5}$/kWh [60] the cost of using firewood increases by around 0.08 €/kWh, leading to a firewood $LCOE$ close to those achieved by the Large system case in the city of Coyhaique.

It is important to note that the thermal load considered for this study does not include domestic hot water (DHW). The inclusion of this additional load is important in further steps, as it represents close to 10% to the total

heat demand in the south of Chile and close to 25% in the central area of the country [2]. The current option for providing DHW in social buildings is through individual liquefied petroleum or natural gas boilers, which work independently from any heating system or appliance. Hence, one alternative to provide DHW with a low emission system is to keep using a system independent from the heating network, such as dedicated rooftop solar collectors. This kind of decentralised system is used in the DLSC project, as a supply temperature of 37°C does not allow to provide DHW from the district heat network without an auxiliar heat source. An alternative could be to use a semi-decentralised system sush as the one proposed by Rehman et al. [18]), using the district network to preheat the DHW plus auxiliar heaters that could increase the temperature of the DHW close to the demand. Lastly, a centralised system could be assessed, with the district network providing the heat for the DHW. This option would require to increase the district network's supply temperature above 50°C, which would increase the thermal loses, but would allow to directly generate domestic hot water and decrease the pumping requirements.

3.3. Optimal angle analysis

The optimal annual yield tilt angle has been extensively analysed in the literature and it is mostly defined by the latitude and the local weather conditions.[62]. However, this optimal annual yield angle is calculated based on maximising the radiation available on the collector's surface, but does not include effects such as thermal losses in the collectors [63], and more importantly, the existence of a demand that would transform the available radiation into useful energy. Particularly, in the case of heating applications,

the mismatch between resource availability and demand (as evident by contrasting figures 1 and 9), leads to optimal tilt angles to deviate from the angle that maximise the annual radiation towards angles that maximise radiation in winter (when the demand is higher). Figure 17 presents the optimal tilt angles (θ) that minimise $LCOE$ and SE for the cases without LTS in both cities. The SF_A in the horizontal axis has been normalised by the total annual demand, which allows to plot the optimal points of the Base and the Large cases together for each city. As a reference, the angles that maximise the annual solar irradiance on the collector have been marked as AO: 29° for Temuco and 34° for Coyhaique; and the angles that maximise the winter solar irradiance on the collector has been marked as WO: 55° for Temuco and 61° for Coyhaique. From Figure 17 it is evident that θ concentrates around WO, with an average of 58.6° for Temuco and 62.4° for Coyhaique. This means that it is worth to have a better performance of the solar collectors in winter, because the demand during June, July and August represents close to 50% of the total annual heating requirements.

Figure 18 presents θ for the configurations in the Pareto front with LTS. Again, the SF_A has been normalised by the total demand in order to present the configurations for the Base and Large case in the same plot. Plots of θ as a function of LTS_{vol} were added to see the effect of the storage capacity on the optimal angle. LTS_{vol} was also normalised by the total annual demand to present the results of both cities aggregated in the same plot.

From Figure 18, it can be appreciated that the average of θ decreases to 50.1° for Temuco and 54.1° for Coyhaique if compared with the cases without LTS (Figure 17). This decrease occurs because the existence of a LTS

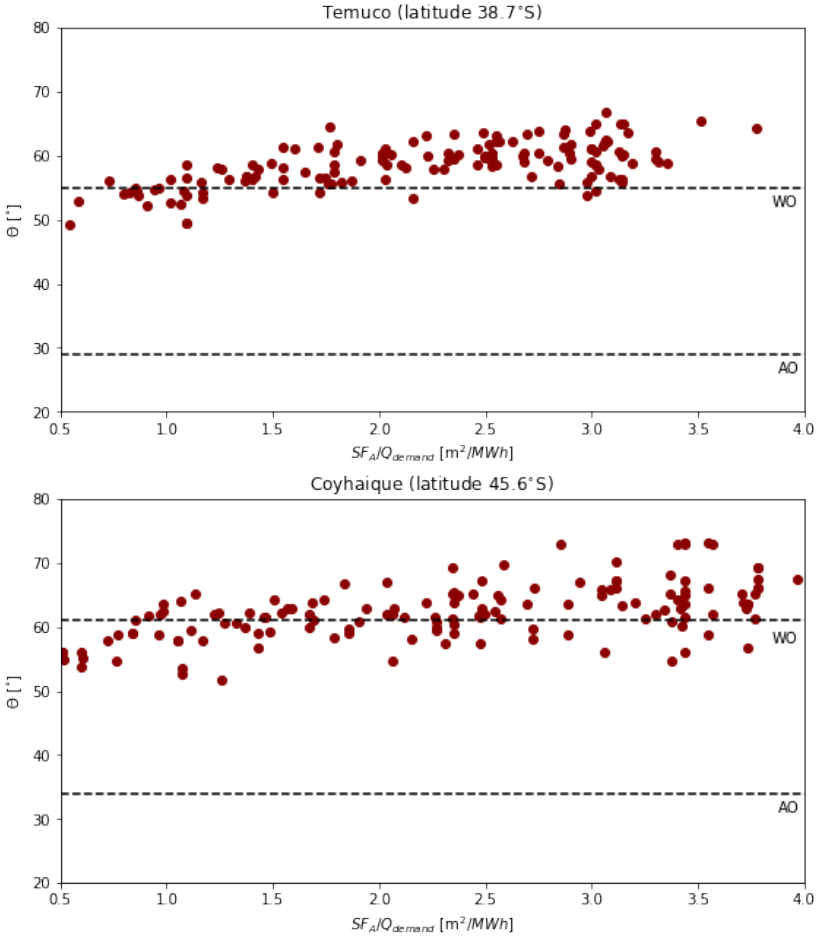

Figure 17: Optimal tilt angles (θ) as a function of SF_A for systems without LTS in the Pareto front in both locations.

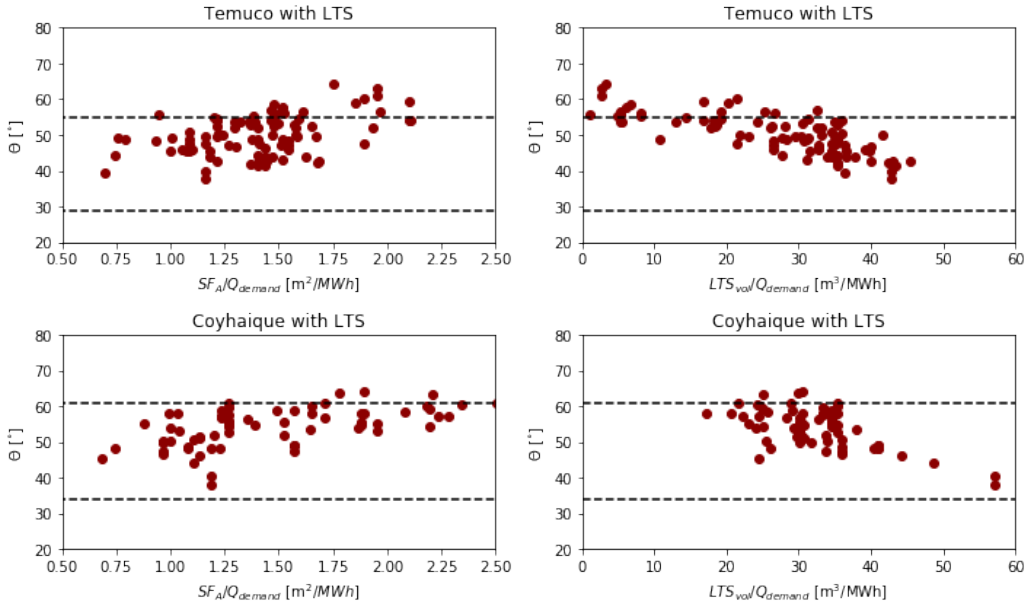

Figure 18: Optimal tilt angles (θ) as a function of SF_A (left) and LTS_{vol} (right) for systems with LTS in the Pareto front in both locations.

allows for shifting part of the energy that could be captured in summer to be used in winter, which favours the use of relatively lower θ. Also, it can be noted that there is a decreasing trend of θ with LTS_{vol}, which means that larger LTS allow a higher percentage of the energy captured in summer to be stored and used in winter, favouring even lower θ. This behaviour explains the big change in θ in Figure 12 at $LCOE$ around 0.12 €/kWh, when the Pareto optimal solutions start including relatively large LTS capacities. This analysis shows that including the tilt angle in the optimisation analysis is relevant, as its correct selection is non trivial and depends on the different characteristics of the solar resource, heat demand and of the relative sizes of the solar field and the storage. It was found that designing the Pareto optimal configurations with the angle that maximises the annual energy on the collector surface (AO) leads to results with on average 1.1% higher $LCOE$ and 14.6% higher SE than the cases with optimised tilt angles. Also, using the angle that maximises the winter energy on the collector surface (WO) leads to on average 0.3% higher $LCOE$ and 1.5% higher SE than optimising the tilt angle for each configuration.

3.4. Optimisation of DH temperature operation

A case with six optimisation variables (SF_A, LTS_{vol}, STS_{vol}, θ, $T_{DH_{sup}}$ and $T_{DH_{ret}}$) was run to compare the effect of optimising the supply ($T_{DH_{sup}}$) and return ($T_{DH_{ret}}$) temperatures of the fluid in cost, emissions and optimal configuration of the system under study.

Figure 19 presents in blue the Pareto front resulting once $T_{DH_{sup}}$ and $T_{DH_{ret}}$ are included as optimisation variables and compares them with the results without optimising the temperature. The colourbar indicates, the ΔT

between $T_{DH_{sup}}$ and $T_{DH_{ret}}$, and points with similar SE ($\overline{T}_{BE}$ and $\overline{C}_{BE}$) and similar $LCOE$ ($\overline{T}_{BC}$ and $\overline{C}_{BC}$) to $\overline{T}_B$ and $\overline{C}_B$ have been highlighted for comparison. Figure 20 presents the values of $T_{DH_{sup}}$ and $T_{DH_{ret}}$ for the points in the Pareto front in both locations, while Figure 21 presents a cost comparison for the points highlighted in Figure 19.

From Figure 19, it is evident that there is an important decrease in $LCOE$ after optimising the temperatures. This reduction reaches around 0.02 €/kWh in Temuco and 0.01 €/kWh in Coyhaique, between 10 and 20% of $LCOE$ decrease. From the colours it is clear that the optimum ΔT between $T_{DH_{sup}}$ and $T_{DH_{ret}}$ is around 17°C for Temuco and 14°C for Coyhaique instead of the 7°C used from the DLSC case. From Figure 20 it can be noted that $T_{DH_{sup}}$ tends to be between 50 and 55°C for Temuco and decreases up to 41°C for Coyhaique. This can be interpreted as higher $T_{DH_{sup}}$ and higher ΔT for the warmer conditions of Temuco, lower $T_{DH_{sup}}$ and ΔT for the cooler conditions in Coyhaique and even lower $T_{DH_{sup}}$ and ΔT (37°C and 7°C, respectively) for the colder conditions of the original DLSC system in Canada.

When comparing $\overline{C}_B$ with $\overline{C}_{BE}$ and $\overline{T}_B$ with $\overline{T}_{BE}$, Figure 21 shows that the main decrease in cost comes from the cost of the pipes, which decreases by 25% for $\overline{C}_{BE}$ and 29% for $\overline{T}_{BE}$, followed by a similar decrease in the cost of the indoor heat delivery system (IHDS). The decrease in the cost of the pipes is explained by the lower flow rate of hot water required to fulfill the demand with a higher ΔT in the DH. Meanwhile, the decrease in the cost of the IHDS is due to the decrease of the area required for the heat exchange when the $LTDS$ increases. This investment decrease is partly compensated

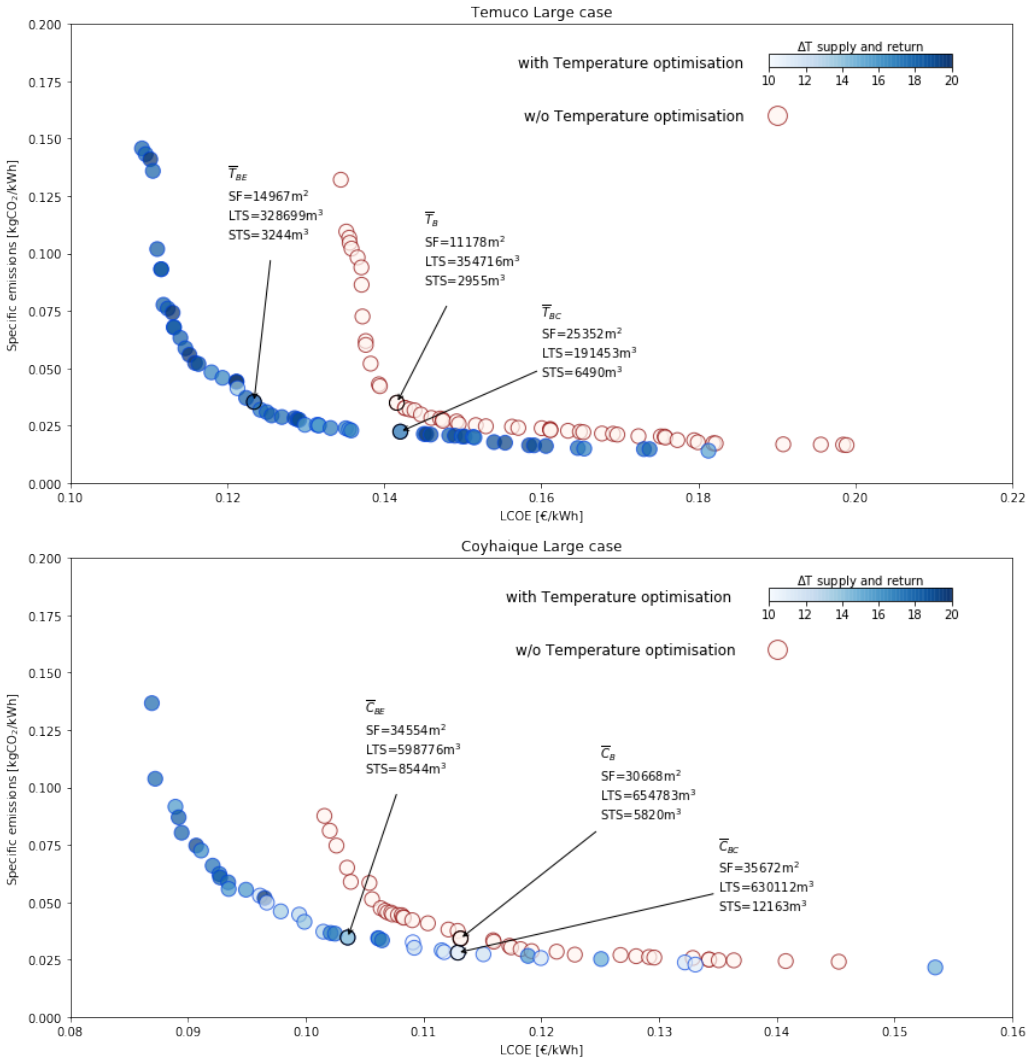

Figure 19: Comparison of Pareto fronts with $T_{DH_{sup}}$ and $T_{DH_{ret}}$ optimised and the case without optimisation ($T_{DH_{sup}}$ and $T_{DH_{ret}}$ constant at the DLSC original value as per equations 2 and 4).

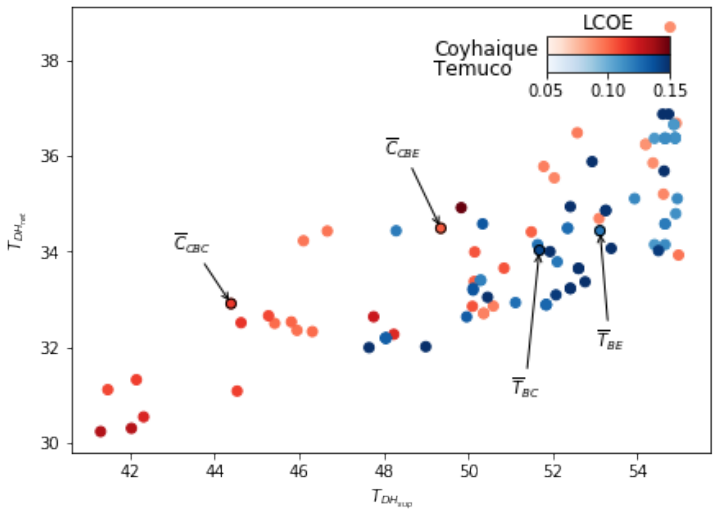

Figure 20: Optimal $T_{DH_{sup}}$ and $T_{DH_{ret}}$ for the different configurations in the Pareto front

by an increase in SF_A and STS_{vol}. In aggregate, the change in investment costs represents the 84% of the total cost decrease for $\overline{C}_{BE}$ and 95% of the decrease for $\overline{T}_{BE}$. The remaining change in $LCOE$ comes from changes in annual operational costs, such as a decrease of the use of electricity (22% for $\overline{C}_{BE}$ and 12% for $\overline{T}_{BE}$) and an increase in the use of fuel (15% for $\overline{C}_{BE}$ and 8% for $\overline{T}_{BE}$). From these changes, the decrease in electricity consumption follows the decrease in water being pumped in the DH, meanwhile the increase in fuel use comes from the higher heat losses in the DH pipes network and from moments when the STS is not able to supply the higher temperature requirements in the DH. Figure 22 presents the increase in heat losses in the DH pipe network due to the increase in the temperature of the water circulating. It is worth to mention that the model considers that the insulation level of the pipes changes when the pipe diameter is modified (according to equation 3), but it is not adjusted for changes in the fluid's temperature

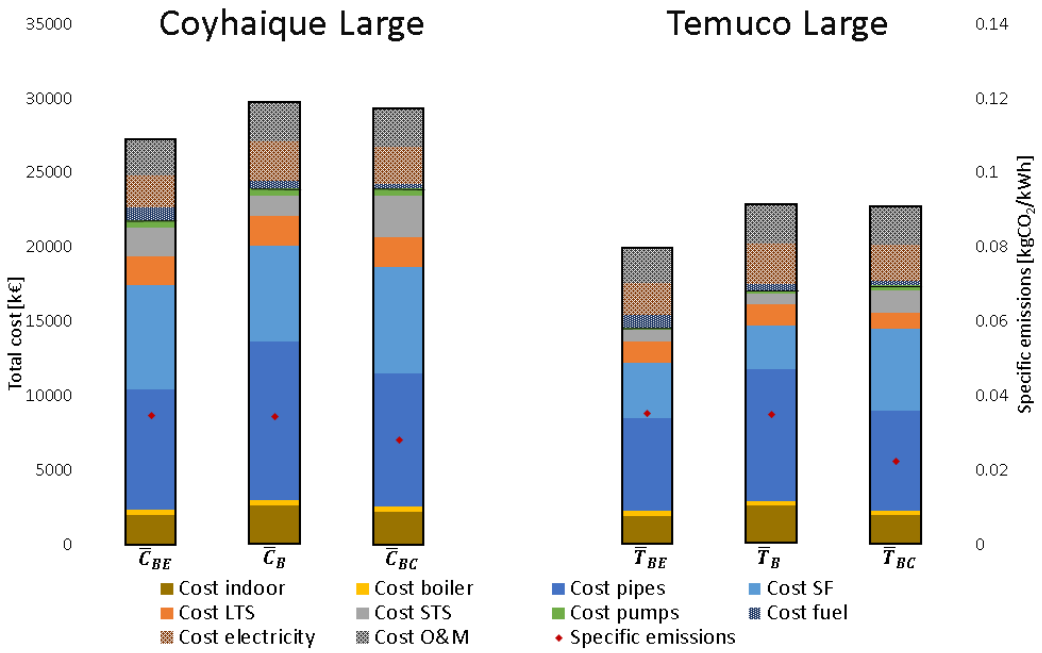

Figure 21: Cost comparison for selected configurations from the Pareto front between optimised and not optimised $T_{DH_{sup}}$ and $T_{DH_{ret}}$. The configurations presented are the same highlighted in Figure 19

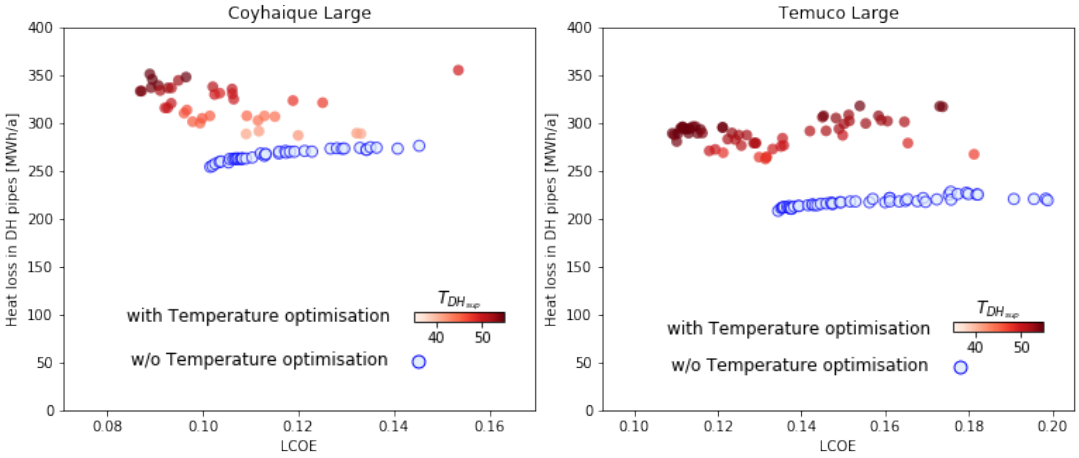

Figure 22: Comparison of the annual thermal losses in the pipes of the DH for the case with and without optimisation of the temperature in both locations

inside the pipe.

3.5. Sensitivity analysis of the model

A sensitivity analysis was performed on the results of the optimisation to evaluate the impact of a variation in the main economic assumptions on the $LCOE$ of the system. To achieve this, the three system configurations highlighted from the Pareto front of the Base and Large case in Figure 11 (C_A, C_B and C_C) and Figure 14 ($\overline{C}_A$, $\overline{C}_B$, $\overline{C}_C$) respectively were analysed. These system configurations were simulated for different electricity costs (C_{elec}), fuel costs (C_{fuel}), investment costs (C_{inv}) and interest rates (r). Each of these parameters was changed by $\pm 10\%$ and $\pm 50\%$ of its original value. The comparison of the $LCOE$ for these sensitivity simulations are presented in Figure 23.

for selected points in the Pareto fronts for the location of Coyhaique in the Base and Large case. On the left axis are presented the parameters that

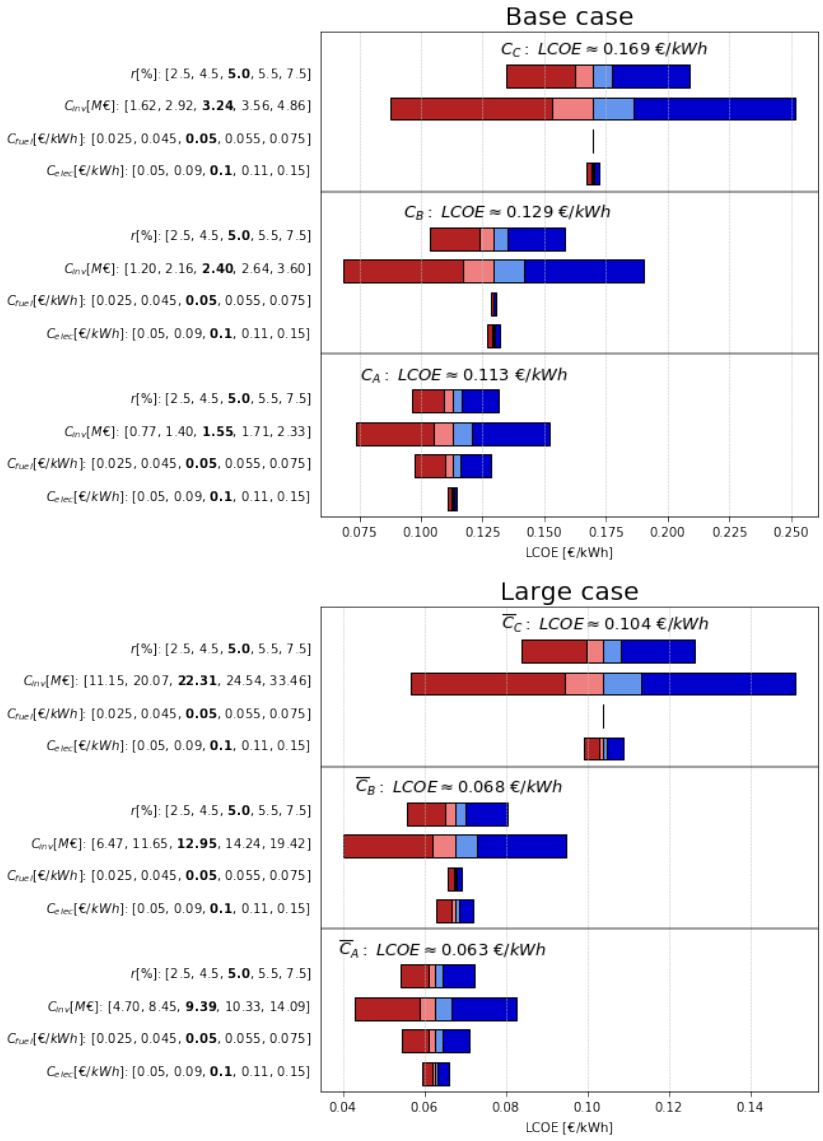

Figure 23: Results of the sensitivity of $LCOE$ to variation in economical parameters.

were changed and the absolute values that were used in the analysis. The bars represent the variation of the $LCOE$ with respect to the case with the original value (in bold).

From the results it can be seen that the $LCOE$ is very sensitive to variations of the investment cost C_{inv} for all cases. This indicates that the system's $LCOE$ is strongly investment cost dependent and that any decrease in the system's capital investment would lead to an almost corresponding decrease in $LCOE$. On the other hand, C_{elec} and C_{fuel} produce relatively low variation in the $LCOE$. A variation of C_{elec} produces higher impact for the Large case, where more pumping is required for water circulation due to a longer piping network. A variation of C_{fuel} produces higher impact in those configurations that have relatively small SFr, such as C_A and $\overline{C}_A$, because these systems require more use of the back-up boiler. The effect of a change in r has also a relatively important impact on the $LCOE$ and, similar to the investment cost C_{inv}, its effect is independent on the size and configuration of the system.

4. Conclusions

As far as the authors are aware, this work develops the first model for multi objective optimisation of a district heating thermal network with seasonal thermal energy storage in the southern hemisphere and under the special cool and sunny conditions in southern Chile. It is also the first that analyses the optimisation of the collector tilt angle considering mismatch between solar resource availability and heat demand and the influence of a long term storage system.

The buildings' demands consider the occupancy rates of average families inhabiting social housing buildings, standard energy gains and air infiltration. The framework simulates the operation of several specific system designs that fulfil the demand combining solar thermal energy and fossil fuel back-up, and uses a genetic algorithm to select and evolve the system designs towards a set of optimal solutions that minimise the $LCOE$ and the specific emissions of the system.

The proposed optimisation framework allows to assess the cost effectiveness of solar thermal networks to decarbonise heat supply. It offers flexibility in managing the design and operation of the system with a high level of detail that allows it to be used in preliminary project design stages, such as feasibility analysis design evaluation and even in early stages of basic engineering design. The result of the optimisation is a set of Pareto optimal solutions that are equivalent from the optimisation perspective. However, the system designer may have other restrictions, such as budget constraints or emission level caps that would be used to select the best design.

The frameworks application to Temuco and Coyhaique shows potential to decrease emissions drastically if compared to a conventional district heating system or to electric heaters. These reductions can be achieved with relatively minor increases in the total cost of the system, reaching 90% emissions decrease by increasing less than 20% the cost for specific optimised system configurations. Furthermore, under certain conditions, this solar district network could be cost-competitive with use of firewood if externalities such as the social costs of local pollution were considered in the economic analysis.

It was shown that the economic and environmental benefits of these sys-

tems can be increased if they are optimised for the local conditions. In particular, it was found that the optimal supply and return temperatures in the district heating network depend on the location of the system, with relatively warmer locations favouring higher supply temperatures and higher differences between supply and return temperature. A correct setting of these operational parameters has impact in both the investment and the operational costs. In the particular case analysed, it leads to total cost decreases of around 10 to 20% when compared with using values from a different location. Also, for the cases analysed, it was found that using an optimised collector tilt angle that considers the existence of a long term storage leads to a decrease in almost 15% in annual emissions and 1% in costs if compared with an angle selected based solely on latitude and 1.5% reduction in annual emissions if compared with an optimal angle that considers the shape of the local thermal demand but does not consider the effect of a long term storage.

The initial investment represents around 70 to 90% of the $LCOE$ of these systems, making them highly sensitive to initial capital finance and the unitary costs of specific elements. In particular, the costs of the piping in the network itself may represent around 40 to 50% of the total investment, and may be affected upward in countries as Chile, where there are no local suppliers nor experience in these technologies. Hence, there is risk of real project costs being higher to those used for this analysis but there is also scope for further cost reductions as the market becomes more mature.

Land cost was not considered in this analysis, as social housing projects are built in state owned land. However, it would be interesting to include a cost for land in the decision process of a private project, as it would tilt the

results towards smaller solar field areas and perhaps larger storage capacities which in the case of borehole thermal energy storage can be underneath other structures.

The $LCOE$ of these systems is sensitive to the scale of the demand and its spatial density. Moreover, as these systems are highly intensive in capital investment, the $LCOE$ is highly sensitive to the load factor and to the investment cost assumed in the model. For the given costs, demand configuration and locations, the results show clearly that the use of seasonal storage could provide extra value to the system. This value, as expected, increases for larger thermal demands (larger networks) and higher demand densities (higher population density). This means that even for small projects, the assessment of possible future growth or interconnection of the system should be considered during the design process.

The minimum emissions of these systems are limited by the indirect emissions of the electricity used by the different pumps. Hence, the minimum achievable emissions tend to increase when the pressure losses in the system increase due to the system increased size, higher buildings or the addition of equipment in the network.

Further research in this field could aim to include domestic hot water demand in the analysis. This would lead to explore other system configurations and potentially increase the value of using higher supply temperature in the district heating network, as this could allow to produce domestic hot water using direct heat from the network.

Nomenclature

$\Delta T_{HX1_{STS}}$	Temperature difference between outlet and inlet on the cold side of the heat exchanger connecting the solar loop with the short term storage [°C]
$\Delta T_{HX2_{DH}}$	Temperature difference between outlet and inlet on the cold side of the heat exchanger connecting the short term storage with the district heating loop [°C]
$\dot{Q}_{boiler}$	Boiler nominal thermal power [kW]
$\dot{Q}_{boiler}$	Thermal power delivered by the boiler [kW]
$\dot{Q}_{fuel}$	Thermal power delivered by the fuel [kW]
$\dot{Q}_{HX2}$	Thermal power through the heat exchanger connecting the short term storage with the district heating loop [kW]
$\dot{Q}_{LTS_{charge}}$	Thermal power discharged from the long term storage [kW]
$\dot{Q}_{LTS_{disch}}$	Thermal power charged to the long term storage [kW]
$\dot{Q}_{pumps}$	Electric power consumed by the pumps [kW]
$\dot{Q}_{SF}$	Thermal power delivered by the solar field [kW]
η_{LTS}	Roundtrip efficiency of the long term storage [-]
η_{Sys}	Efficiency of the system using the solar energy collected in the solar field
C_{elec}	Electricity cost from running the pumps [€/a]

C_{fuel}	Fuel cost from running the boiler [€/a]
C_{inv}	Investment cost [€]
C_{OM}	Operation and maintenance cost [€/a]
D_{pipe}	Pipe diameter [m]
EF_{fuel}	Emission factor of the fuel [kgCO_2/kWh]
EF_{grid}	Emission factor of the electric grid [kgCO_2/kWh]
G	Global irradiance on the collector's surface [kJ/h·m^2]
I_{pipe}	Pipe's heat transfer coefficient considering insulation [kJ/h·m^2·K]
$LCOE$	Levelized cost of energy [€/kWh]
$LMTD$	Logarithmic mean temperature difference [°C]
LTS_{vol}	Long term storage volume [m^3]
Q_{load}	Total annual demand of the load connected to the district network [kWh/a]
r	Discount rate [-]
SE	Specific emission per unit of energy provided by the heating system [kgCO_2/kWh]
SF_A	Solar field area [m^2]
SFr	Solar fraction [-]

STS_{vol}	Short term storage volume [m^3]
$T_{DH_{ret}}$	Setpoint temperature to the return water of the district heating network [°C]
$T_{DH_{sup}}$	Setpoint temperature of the supply water fed to the district heating network [°C]
T_{ext}	External/ambient temperature [°C]
T_{int}	Temperature inside the building [°C]
$T_{LTS_{avg}}$	Average temperature across the long term storage [°C]
$T_{LTS_{ctr}}$	Temperature at the centre pf the long term storage [°C]
$T_{SF_{in}}$	Inlet temperature to the solar collector [°C]
$T_{SF_{out}}$	Outlet temperature from the solar collector [°C]
$T_{STS_{btm}}$	Lowest temperature in the short term storage / temperature at the bottom of the cold short term storage tank [°C]
$T_{STS_{top}}$	Highest temperature in the short term storage / temperature at the top of the hot short term storage tank [°C]
v_{max}	Maximum flow velocity allowed in the pipe [m/s]

Appendix A. Building envelope materials

Table A.12: Building envelope material in the city of Temuco

Surfaces	Material	Temuco		
		Thickness [mm]	Density [kg/m^3]	Thermal conductivity [W/mK]
External wall	Lightweight concrete	20	800	0.26
	Brick	175	1000	0.46
Boundary wall	Cement mortar	10	2000	1.40
	Brick	140	1000	0.46
	Cement mortar	10	2000	1.40
Internal wall	Wall board	50	600	0.29
Internal ceiling/floor	Lightweight concrete	120	800	0.26
	Linoleum	4	1000	1.02
External roof	Ceiling board	10	600	0.29
	Polystyrene	40	20	0.03
	Fiber cement	4	1250	0.23
Ground	Common cement	200	2400	2.10
	Linoleum	4	1000	1.02
Windows	Glass	5	2500	0.9

Table A.13: Building envelope material in the city of Coyhaique.

Surfaces	Material	Temuco		
		Thickness [mm]	Density [kg/m^3]	Thermal conductivity [W/mK]
External wall	Polystyrene	40	20	0.03
	Brick	175	1000	0.46
Boundary wall	Cement mortar	10	2000	1.40
	Brick	140	1000	0.46
	Cement mortar	10	2000	1.40
Internal wall	Wall board	50	600	0.29
Internal ceiling/floor	Lightweight concrete	120	800	0.26
	Linoleum	4	1000	1.02
External roof	Ceiling board	10	600	0.29
	Polystyrene	120	20	0.03
	Fiber cement	4	1250	0.23
Ground	Common cement	200	2400	2.10
	Linoleum	4	1000	1.02
Windows	Glass	5	2500	0.9

References

[1] International Energy Agency, Perspective for the Clean Energy Transition - the Critical Role of Buildings, Technical Report, 2019.

[2] S. Tolvett, Futuro de la calefacción en Chile: Opciones y Consecuencias, Technical Report, 2015.

[3] C. Yáñez, A. Fissore, A. Leiva, Informe final de usos de la energía de los hogares Chile 2018, Technical Report, CDT, 2019.

[4] Ministerio del Medio Ambiente, Cuarto Reporte del Estado del Medio Ambiente, Technical Report, Santiago, Chile, 2018.

[5] International Energy Agency, Renewables 2019: Analysis and forecast to 2024, Technical Report, 2019.

[6] A. Hast, S. Syri, V. Lekavičius, A. Galinis, District heating in cities as a part of low-carbon energy system, Energy 152 (2018) 627–639. doi:10.1016/j.energy.2018.03.156.

[7] V. M. Soltero, R. Chacartegui, C. Ortiz, R. Velázquez, Evaluation of the potential of natural gas district heating cogeneration in Spain as a tool for decarbonisation of the economy, Energy 115 (2016) 1513–1532. doi:10.1016/j.energy.2016.06.038.

[8] A. Castillejo-Cuberos, R. Escobar, Understanding solar resource variability: An in-depth analysis, using Chile as a case of study, Renewable and Sustainable Energy Reviews 120 (2020) 109664. doi:10.1016/j.rser.2019.109664.

[9] A. Molina, M. Falvey, R. Rondanelli, A solar radiation database for Chile, Scientific Reports 7 (2017) 1–11. doi:10.1038/s41598-017-13761-x.

[10] A. Urquiza, C. Amigo, M. Billi, T. Leal, P. Araya, A. Cortés, I. Rivas, M. Valdés, F. Valencia, Analisis de fuentes secundarias disponibles de alcance nacional, Technical Report, 2017.

[11] A. Cortés, I. Ridley, Efectos de la combustión a leña en la calidad del aire intradomiciliario. La ciudad de Temuco como caso de studio, Revista INVI 28 (2014) 257–271. doi:10.4067/s0718-83582013000200008.

[12] A. Sorensen, Solar district heating guidelines, Technical Report, Planenergi, 2012.

[13] R. Krug, V. Mehrmann, M. Schmidt, Nonlinear optimization of district heating networks, Optimization and Engineering (2020) 1–37. doi:10.1007/s11081-020-09549-0.

[14] L. Blackburn, A. Young, P. Rogers, J. Hedengren, K. Powell, Dynamic optimization of a district energy system with storage using a novel mixed-integer quadratic programming algorithm, Optimization and Engineering 20 (2019) 575–603. doi:10.1007/s11081-018-09419-w.

[15] D. Romanchenko, E. Nyholm, M. Odenberger, F. Johnsson, Impacts of demand response from buildings and centralized thermal energy storage on district heating systems, Sustainable Cities and Society 64 (2021). doi:10.1016/j.scs.2020.102510.

[16] R. Renaldi, D. Friedrich, Techno-economic analysis of a solar district heating system with seasonal thermal storage in the UK, Applied Energy 236 (2019) 388–400. doi:10.1016/j.apenergy.2018.11.030.

[17] Natural Resources Canada, Drake landing solar community, 2020. URL: `https://www.dlsc.ca/`.

[18] H. u. Rehman, J. Hirvonen, K. Sirén, Performance comparison between optimized design of a centralized and semi-decentralized community size solar district heating system, Applied Energy 229 (2018) 1072–1094. doi:10.1016/j.apenergy.2018.08.064.

[19] J. Lizana, R. Chacartegui, A. Barrios-Padura, J. M. Valverde, Advances in thermal energy storage materials and their applications towards zero energy buildings: A critical review, Applied Energy 203 (2017) 219–239. doi:10.1016/j.apenergy.2017.06.008.

[20] S. K. Shah, L. Aye, B. Rismanchi, Multi-objective optimisation of a seasonal solar thermal energy storage system for space heating in cold climate, Applied Energy 268 (2020) 115047. doi:10.1016/j.apenergy.2020.115047.

[21] Gobierno de Chile, Reglamentacion Termica - Manual de aplicacion, Technical Report, Santiago, Chile, 2006. doi:10.16258/j.cnki.1674-5906.2006.01.022.

[22] S. Navarrete, Infiltraciones de Aire en la Vivienda., Ph.D. thesis, Universidad de Concepción, 2016.

[23] M. Diaz, Evaluación de impacto de mejoras aplicadas a la hermeticidad al aire y aislación térmica para la verificación de la eficiencia energética mediante simulación térmica dinámica de dos viviendas tipo en Concepción, Ph.D. thesis, 2015.

[24] T. Kusuda, M. Mizuno, J. Bean, Seasonal Heat Loss Calculation for Slab-On-Grade Floors (1982). doi:10.6028/NBS.IR.81-2420.

[25] (CR)2, Exolorador climático, 2016. URL: http://explorador.cr2.cl/.

[26] M. Reuss, The use of borehole thermal energy storage (BTES) systems, in: Advances in Thermal Energy Storage Systems: Methods and Applications, Elsevier Inc., 2014, pp. 117–147. doi:10.1533/9781782420965.1.117.

[27] G. Hellström, Ground heat storage : thermal analyses of duct storage systems, Ph.D. thesis, Lund University, Lund, 1991.

[28] M. Mella, D. Quiroz, Geología del área de Temuco-Nueva Imperial, Serie de geología basica 122 (2010).

[29] R. de la Cruz, M. Suarez, M. Belmar, D. Quiroz, M. Bell, Geologia del area Coihaique - Balmaceda, Serie de geología basica 80 (2003).

[30] H. J. Quintana, M. Kummert, Optimized control strategies for solar district heating systems, Journal of Building Performance Simulation 8 (2015) 79–96. doi:10.1080/19401493.2013.876448.

[31] V. Masatin, E. Latõšev, A. Volkova, Evaluation Factor for District Heating Network Heat Loss with Respect to Network Geometry, Energy Procedia 95 (2016) 279–285. doi:10.1016/j.egypro.2016.09.069.

[32] L. Zeghadnia, J. L. Robert, B. Achour, Explicit solutions for turbulent flow friction factor: A review, assessment and approaches classification, 2019. doi:10.1016/j.asej.2018.10.007.

[33] L. Yang, E. Entchev, A. Rosato, S. Sibilio, Smart thermal grid with integration of distributed and centralized solar energy systems, Energy 122 (2017) 471–481. doi:10.1016/j.energy.2017.01.114.

[34] Ministerio de Desarrollo Social, Metodologogia de preparacion y evaluacion proyectos de edificacion publica, Technical Report, 2013.

[35] G. Edwards, Estimacion de la tasa docial de descuento a largo plazo en el marco de los sistemas nacionales de inversion - Aplicacion al caso chileno, El trimestre economico LXXXIII (2016) 99–125.

[36] F. Mauthner, S. Herkel, Technology and demonstrators - Technical Report Subtask C – Part C1, Technical Report January, 2016.

[37] Intergas, Informativo tarifas Temuco, 2019. URL: https://www.intergas.cl/docs/InformativoTarifasTemuco.pdf.

[38] Comision Nacional de Energia, Mapa Precio de Combustibles – Energía Abierta — Comisión Nacional de Energía, 2020. URL: http://energiaabierta.cl/visualizaciones/mapa-precio-de-combustibles/.

[39] CGE, Tarifas de suministro, 2020. URL: https://www.cge.cl/wp-content/uploads/2020/01/Tarifas-de-Suministro-CGE-Enero-2020.pdf.

[40] Saesa, Tarifas Vigentes, 2020. URL: https://www.gruposaesa.cl/edelaysen/tarifas-vigentes/.

[41] Planenergi, Best practice for implementation and operation of large sale borehole and pit heat thermal storage, Technical Report, 2019.

[42] T. Nussbaumer, S. Thalmann, Influence of system design on heat distribution costs in district heating, Energy 101 (2016) 496–505. doi:10.1016/j.energy.2016.02.062.

[43] P. Voll, Automated optimization-based synthesis of distributed energy supply systems, Ph.D. thesis, Aachen University, 2013.

[44] Ministerio de Energía, Proceso de Planificación Energética de Largo Plazo, Technical Report, 2017.

[45] Defra, Greenhouse gas reporting: conversion factors 2020 - GOV.UK, 2020. URL: https://www.gov.uk/government/publications/greenhouse-gas-reporting-conversion-factors-2020.

[46] T. Estay, X. Ovalle, Desarrollo de factores de emisión específicos para el programa HuellaChile, Technical Report, Universidad Andres bello, 2017.

[47] F.-A. Fortin, U. Marc-André Gardner, M. Parizeau, C. Gagné, DEAP:

Evolutionary Algorithms Made Easy François-Michel De Rainville, Journal of Machine Learning Research 13 (2012) 2171–2175.

[48] Deap Project, DEAP documentation — DEAP 1.3.1 documentation, 2020. URL: `https://deap.readthedocs.io/en/master/index.html`.

[49] A. Hassanat, K. Almohammadi, E. Alkafaween, E. Abunawas, A. Hammouri, V. B. S. Prasath, Choosing Mutation and Crossover Ratios for Genetic Algorithms—A Review with a New Dynamic Approach, Information 10 (2019) 390. doi:10.3390/info10120390.

[50] Ministerio de Vivienda y Urbanismo, Calificación energética de viviendas, Technical Report, 2018. URL: `www.calificacionenergetica.cl`.

[51] W. Bustamante, R. Cepeda, P. Matrinez, H. Santa Maria, Eficiencia energética en vivienda social: un desafío posible, Technical Report, 2009.

[52] K. Sipilä, M. Rämä, H. Zinko, U. Ottosson, J. Williams, A. Aguiló-Rullán, B. Bøhm, District heating for energy efficient building areas, Technical Report, 2011.

[53] F. Jalil-Vega, A. D. Hawkes, Spatially resolved model for studying decarbonisation pathways for heat supply and infrastructure trade-offs, Applied Energy 210 (2018) 1051–1072. doi:10.1016/j.apenergy.2017.05.091.

[54] I. Dochev, I. Peters, H. Seller, G. K. Schuchardt, Analysing district heating potential with linear heat density. A case study from Hamburg., in: Energy Procedia, volume 149, Elsevier Ltd, 2018, pp. 410–419. doi:10.1016/j.egypro.2018.08.205.

[55] Heat network partnership for Scotland, District Heating Strategy Fact-sheet, Technical Report, 2017.

[56] F. Morales, C. De, C. Roger, W. B. Eggen, M. Henríquez, Manual de desarrollo de proyectos de energia distrital, Technical Report, EBP, Santiago, 2018.

[57] T. Schmidt, D. Mangold, H. Müller-Steinhagen, Central solar heating plants with seasonal storage in Germany, Solar Energy 76 (2004) 165–174. doi:10.1016/j.solener.2003.07.025.

[58] S. Hsieh, A. Omu, K. Orehounig, Comparison of solar thermal systems with storage: From building to neighbourhood scale, Energy and Buildings 152 (2017) 359–372. doi:10.1016/j.enbuild.2017.07.036.

[59] F. Mauthner, S. Herkel, Technical Report Subtask C – Part C1 (2016) 1–31.

[60] Ambiente Consultores, Análisis del mercado y estimación del impacto energético, económico, social y ambiental de fijar un estándar mínimo de eficiencia energética en artefactos que consumen leña y otros dendroenergéticos, Technical Report, Ministerio de Energía, 2013.

[61] Chile Ambiente, Estudio de Análisis del Potencial Estratégico de la Leña en la Matriz Energética Chilena, Technical Report, Comision Nacional de Energia, 2008.

[62] M. Chinchilla, D. Santos-Martín, M. Carpintero-Rentería, S. Lemon, Worldwide annual optimum tilt angle model for solar collectors and

photovoltaic systems in the absence of site meteorological data, Applied Energy 281 (2021) 116056. doi:10.1016/j.apenergy.2020.116056.

[63] Y. Lv, P. Si, X. Rong, J. Yan, Y. Feng, X. Zhu, Determination of optimum tilt angle and orientation for solar collectors based on effective solar heat collection, Applied Energy 219 (2018) 11–19. doi:10.1016/j.apenergy.2018.03.014.